https://doi.org/10.1016/j.tws.2020.107298

Design of lean duplex stainless steel tubular sections subjected to concentrated end bearing loads at elevated temperatures

Yancheng Cai [a], Feng Zhou [b,c*], Liping Wang [d] and Ben Young [a]

[a] Department of Civil and Environmental Engineering, The Hong Kong Polytechnic University, Hong Kong, China
(Formerly, Department of Civil Engineering, The University of Hong Kong, Pokfulam Road, Hong Kong, China)
[b] Department of Structural Engineering, Tongji University, 1239 Siping Road, Shanghai 200092, China
[c] State Key Laboratory of Disaster Reduction in Civil Engineering, Tongji University, Shanghai 200092, China
[d] School of Civil Engineering, Central South University, Changsha, Hunan Province, China

Abstract

Design rules for web crippling of stainless steel tubular sections at elevated temperatures are currently unavailable. In this study, non-linear finite element models (FEMs) were developed for the web crippling of cold-formed lean duplex stainless steel (CFLDSS) square and rectangular hollow sections under the concentrated end bearing loads, namely the loading conditions of End-One-Flange (EOF), End-Two-Flange (ETF) and End Loading (EL). After successful validation of the FEMs, an extensive parametric study of 210 CFLDSS tubular sections at elevated temperatures (up to 950 °C) was performed. The appropriateness of the web crippling design rules in the current international specifications and literature was examined by comparing their ultimate strength predictions with those obtained from the parametric study. The material properties at room (ambient) temperature condition were substituted by those at elevated temperatures. It was found that the predictions by the current design specifications and the literature were generally unconservative and not reliable, while the European Code provided reliable but generally very conservative predictions. A new design method by using the Direct Strength Method was proposed for the web crippling of CFLDSS tubular sections at elevated temperatures under the loading conditions of EOF, ETF and EL. The assessments indicated that the predictions by using the new method were generally conservative and reliable.

Keywords: Concentrated bearing loads, direct strength method, elevated temperatures, lean duplex stainless steel, finite element analysis, web crippling.

* Corresponding author.
E-mail address: zhoufeng@tongji.edu.cn (F. Zhou).

1 Introduction

The alloying elements of stainless steel have been developing since its invention, with the aim of providing better mechanical properties, and higher corrosion resistance or oxidation resistance in the case of high temperature application [1]. The relatively new stainless steel, lean duplex stainless steel (such as EN 1.4062 and EN 1.4162), is a high strength material with nominal 0.2% proof stress of 450 MPa. It has economic advantages over the other types of conventional stainless steel due to the much lower nickel content, around 1.5%. Furthermore, it still possesses the material properties as those of conventional stainless steels. Hence, it is becoming an attractive choice as a construction material in civil and structural engineering industry, for example, it is used in the footbridge in Siena [2]. It should be noted that the lean duplex stainless steel is not covered in the current American (ASCE) [3]) and Australian/New Zealand (AS/NZS) [4] stainless steel design specifications, while it was recently introduced in the European Code (EN 1993-1-4) [5].

Over the last decade, significant progress has been made to understand its structural performance and subsequently the design criteria of lean duplex stainless steel. This could be viewed from the fundamental material properties by the tensile coupon tests [6,7], and structural members, such as beams [7,8], columns [9-11], plate girders [12,13], and the connections by bolts [14]. In these investigations, the design rules in the stainless steel specifications of ASCE [3], AS/NZS [4] and European Code [15] were assessed. Efforts were also made when necessary to propose modified design equations and new design methods for the better strength predictions of lean duplex stainless steel structures. It should be noted that these investigations were conducted at room (ambient) temperature condition, but not at elevated temperatures.

Many research works have been carried out for the structural behaviour and design of carbon steel members at elevated temperatures [16-22]. It has been recognized that stainless steel generally exhibits better retention of strength and stiffness in comparison with carbon steel at elevated temperatures, and such superior characteristics have been utilised in high temperature industrial applications for many years [23]. In the last few years, attention has been received to investigate the structural performance and develop the design rules for stainless steel structures at elevated temperatures, for examples, the beams [24] and tubular joints [25] that fabricated by austenitic stainless steel (EN 1.4301) and duplex stainless steel (EN 1.4462), as well as bolted connections that fabricated by lean duplex stainless steel (EN 1.4162) [26-29].

Web crippling is a form of localised buckling that generally occurs near the points of concentrated loads or supports of structural members. Cold-formed stainless steel tubular sections that are unstiffened against this type of loading could be critical, and thus the failure of web crippling must be carefully checked. The web crippling design rules for cold-formed stainless steel structures in

current specifications [3-5] are generally empirical in nature and are based on those for cold-formed carbon steel [30]. It has been found that the current design rules are generally not able to provide accurate and reliable predictions for the web crippling strengths of stainless steel members [31-36]. Note that the material properties of stainless steel differ from those of carbon steel, for example, at room temperature condition, it displays a more rounded stress-strain response with a higher ratio of ultimate-to-yield stress and greater ductility when compared to carbon steel [23].

Recent experimental investigations of over 100 cold-formed lean duplex stainless steel (CFLDSS) tubular members undergoing web crippling were carried out by Cai and Young [37,38]. It showed that the strengths predicted by the current stainless steel [3-5] and carbon steel [39] design specifications, as well as the design rules in the literature [40] were generally conservative. It should be noted that the design of lean duplex stainless steel members at elevated temperatures has not been covered in the current international stainless steel design codes [3-5]. A search of the literature revealed a lack of research on web crippling of CFLDSS members at elevated temperatures. In this study, the structural behaviour and design of CFLDSS tubular sections subjected to web crippling at elevated temperatures were investigated by using finite element analysis. The experiments conducted by Cai and Young [37] were used to develop the finite element models (FEMs). The sections were under the loading conditions of End-One-Flange (EOF), End-Two-Flange (ETF) and End Loading (EL) at the elevated temperatures ranged from 22 to 950 °C. The web crippling design rules at room temperature condition in the current design specifications [3-5, 39] were examined for the possibility of application at elevated temperature conditions. In doing so, the reduced material properties at elevated temperatures were used in calculating the web crippling strengths. Furthermore, the web crippling design rules in literature for room temperature condition were also assessed for elevated temperatures in this study. Finally, a new design method by using the Direct Design Method (DSM) for elevated temperature conditions is proposed.

2 Summary of test program

The tests of CFLDSS tubular sections subjected to web crippling failure under concentrated end bearing loads (EOF, ETF and EL) were presented in Cai and Young [37]. These tests were conducted at room temperature condition. The test results provided the test strengths, load-deformation curves and failure modes of the sections. It should be noted that the loading conditions of EOF and ETF referred to those specified in the current stainless steel design specifications, such as ASCE [3] and AS/NZS [4]; while the EL condition simulated the floor joist members positioned on a solid foundation under concentrated end bearing load.

The CFLDSS had square and rectangular hollow sections ($H \times B \times t$) with grade EN 1.4062 (AISI S32202). Figure 1 illustrates the definition of the symbols in a CFLDSS section, where H and h are the overall height and the flat portion of the section web, respectively; B and t are the respective width and thickness of the section. The material properties of the CFLDSS at room temperature condition were obtained by tensile flat coupon tests. The material properties obtained from the tensile flat coupons that extracted in the longitudinal direction of the sections are summarized in Table 1, including the Young's modulus (E_r), 0.2% proof stress ($f_{0.2,r}$) and ultimate stress ($f_{u,r}$) at room temperature. Details of the coupon tests are described in Cai and Young [37].

The aforementioned CFLDSS tubular members were used to fabricate the test specimens under concentrated end bearing loads. The test strengths (P_t) of CFLDSS specimens for the numerical verifications are shown in Table 2. The specimens were tested under the loading conditions of EOF, ETF and EL. The specimen labels are generally identified by the loading condition, section dimension and the bearing length. For example, the label of specimen EOF120×60×3.0N60, where the "EOF" indicates the loading condition of "End-One-Flange"; the following term "120×60×3.0" means the section dimension of "$H \times B \times t$" in the unit of mm; and the notation "N60" indicates the loading plate with bearing length of 60 mm (N = 60 mm) was used in the test. If it is a repeated specimen, the segment of "-r" was followed in the last part of the specimen label, e.g., the repeated specimen ETF100×100×3.0N90-r. Displacement control test method was used by driving the hydraulic actuator with a constant loading rate of 0.3 mm/min for all test specimens. The test setup of the EOF, ETF and EL conditions are illustrated in Figure 2. The details of the testing procedures are described in Cai and Young [37].

3 Finite element models

3.1 General

The FEMs using the ABAQUS program of version 6.20 [41] were developed to simulate the aforementioned web crippling tests of CFLDSS specimens. Three main components in the tests were modelled, namely, the steel bearing plates, the CFLDSS specimen, and the interaction between the steel bearing plates and CFLDSS specimen. In the FEMs, the measured dimensions and tested stress-strain curves of CFLDSS [37] were used. In addition, the corners of the CFLDSS sections were carefully modelled. These will be described in the following sections. The results obtained from the finite element analysis (FEA) were compared with the test results [37] in terms of ultimate strengths, failure modes and load-deformation curves.

3.2 Element types and mesh sizes

The shell element type S4R that is a four-node doubly curved element with reduced integration and hourglass control was selected to simulate the CFLDSS tubular specimens. The S4R element has six degree of freedom per node and is suitable for complex buckling behaviour as mentioned in the ABAQUS manual [41]. The element S4R has been adopted in the FEMs to successfully simulate the web crippling behaviour of duplex stainless steel [30] and ferritic stainless steel [32,33] tubular members. The CFLDSS members were modelled based on the centreline dimensions of the cross-sections. The solid element type C3D8R was selected to simulate the steel bearing plates. The steel bearing plates were defined as rigid body as these plates in the test program [37] were very thick, and were fabricated by high strength steel which had much higher yield strength than those of the CFLDSS specimens. The mesh sizes in the flat portions of the cross-sections ranged from 2×2 mm to 10×10 mm (length by width) depending on the dimension of the cross-sections. Similar mesh sizes were adopted on the basis of the sensitivity study for the FEMs of austenitic and duplex stainless steel [30] and ferritic stainless steel [32,33] tubular members subjected to web crippling. A finer mesh size at the round corners was adopted in order to consider the influence of the corner radius more accurately [32-34, 42].

3.3 Material properties

The ABAQUS [41] allows for the multi-linear stress-strain curves to be used in the input of material properties. The engineering stress-strain curves obtained from the tensile coupon tests [37] were used. Since the web crippling behaviour of CFLDSS involves locally large in-elastic strains, the engineering stress-strain (σ-ε) curve was converted to a true stress (σ_{true}) and logarithmic plastic strain (ε_{true}^{pl}) curve, by using the following Equations (1)-(2):

$$\sigma_{true} = \sigma(1 + \varepsilon) \quad (1)$$

$$\varepsilon_{true}^{pl} = ln(1 + \varepsilon) - \frac{\sigma_{true}}{E} \quad (2)$$

where E is the measured Young's modulus. The true stress and logarithmic plastic strain curve was then mimicked by means of a piecewise linear stress-strain model, in particular, over the strain-hardening region. Hence, the material non-linearity was incorporated into the FEMs. The tensile material properties (Table 1) [37] were assigned to the webs and flanges of the sections.

3.4 Boundary conditions

The boundary conditions in the FEMs were modelled in accordance with the tests. Half of the CFLDSS specimens and steel bearing plates were considered in the FEMs by assigning appropriate symmetric boundary conditions. This is because the geometries and failure modes of the test specimens

were generally in a symmetric manner. Furthermore, the test setups with the boundary conditions are symmetric for the loading conditions of EOF, ETF and EL [37]. The interfaces between the CFLDSS sections and the steel bearing plates were modelled using the contact pairs, with the steel bearing plates defined as master surface while the CFLDSS sections as slave surface. The contact surfaces were defined as "hard contact" in the normal direction and were not allowed to penetrate each other. In the tangential direction, a coefficient of 0.4 was used to consider the friction penalty contact [32,33]. Proper boundary conditions were assigned to the reference points (RPs) of the steel bearing plates to simulate the roller support and half round support in the test setup. For examples, the boundary conditions of $U_x = 0$, $U_z = 0$, $R_y = 0$ and $R_z = 0$ (R_y and R_z mean the rotation about the Y and Z axes, respectively) were assigned to RP-1 (see Fig. 3) of the bearing plate to simulate the half round support. Similar to the test setup, in the FEM, the out-of-plane deformation of the flat webs at mid-span was restrained ($U_x = 0$, where U_x means translation in the X direction, as shown in Fig. 3) by a length equal to the width of the steel bearing plate (Fig. 2(a)**)**. The geometrical nonlinearity of the FEMs was considered by the NLGEOM command in ABAQUS [41].

3.5 Method of loading

The loading method used in the analysis of the FEMs of CFLDSS was identical to that used in the test program, where displacement control test method [37] was adopted. The compressive load was applied by specifying a displacement to the reference point of the analytical rigid plate that simulate the steel bearing plate. The contact pairs were performed before applying the compressive load. Generally, the contacts were analysed in two steps. The static analysis method in ABAQUS program was used in the analysis. The comparison of the tests and FEMs for CFLDSS specimens subjected to different concentrated end bearing loads are illustrated in Figures 4-6, for specimens of EOF80×150×3.0N90, ETF150×80×3.0N90 and EL100×100×3.0N90, respectively.

4 Validation of finite element models

In the verification of the FEMs, a total of 36 CFLDSS tubular sections tested by Cai and Young [37] at room temperature condition were analysed in this study. These specimens failed by web crippling under the loading conditions of EOF, ETF and EL (Table 2). The web crippling strengths (P_t) per web obtained from the test program were compared with those obtained from the numerical results ($P_{FEA,r}$), as shown in Table 2. Table 3 summarizes the mean value of the $P_t/P_{FEA,r}$ for the three different loading conditions. Overall, the mean value of the $P_t/P_{FEA,r}$ for the 36 specimens is 1.04 with the corresponding coefficient of variation (COV) of 0.086. The test strengths are overall a little bit higher than the predicted strengths from the FEA. The failure modes observed from the tests were also

well predicted by the FEA for the three different loading conditions, as illustrated in Figures 4-6. Figure 7 further illustrates the comparisons of the applied load versus the vertical web deformation curves obtained from the tests and FEA, for specimens of EL100×100×3.0N90, EL150×80×3.0N90 and ETF60×40×3.0N30. In summary, the comparisons indicated that generally, both the failure modes and the ultimate web crippling strengths obtained from the test program could be replicated by the developed FEMs.

5 Parametric study analysis and discussions

After successful validation of the FEMs, the validated FEMs were used to generate numerical data for the CFLDSS tubular sections under the concentrated end bearing loads (EOF, ETF and EL) at elevated temperatures. A total of 210 specimens at elevated temperatures were analysed in the parametric study, and these temperatures were 22 (room temperature), 200, 350, 500, 600, 800 and 950 °C. The CFLDSS tubular sections were carefully designed by considering the key parameters in the web crippling design rules [3-5] for steel tubular sections. The tubular sections included five rectangular and five square hollow sections (H×B×t). The key parameters in these sections were designed, including the ratios of h/t ranged from 21.0 to 145.0, N/t ranged from 8.3 to 125.0 and N/h ranged from 0.36 to 1.24. The section inner corner radius (r) for each specimen was designed based on handbook of the supplier. The radio of r/t either equal to 1.0 or 1.5 was used. In each loading condition (EOF, ETF or EL), each section was loaded by two different bearing lengths (N), i.e., either $N = 0.5B$ or $N = 1.0B$. The details of these sections and key parameters are presented in Table 4. The labelling system for the specimens in the parametric study is identical to that used in the test program as described in the Section 2 of this paper.

The stress-strain curves of the tensile flat coupons in the longitudinal direction of CFLDSS (grade EN 1.4162) rectangular section at elevated temperatures were used in the parametric study. These stress-strain curves at elevated temperatures were measured by Cai and Young [26] using steady state test method. It should be noted that the stress-strain curves at the corner regions of the CFLDSS section may differ from those in the flat regions due to the effect of cold-working. The enhancements in $f_{0.2\%}$ are found to be obvious in the corners of cold-formed sections [43] at room temperature condition. However, the material properties from corner and flat portions display similar $f_{0.2\%}$ at high temperature conditions [44]. Since the web crippling failure occurred in the web for the CFLDSS tubular sections in the parametric study, the enhancements of the corner regions had little effects on the ultimate web crippling capacity. In this sense, the enhancements of the strengths at the corner regions were not considered in the present study, as those studied by Feng and Young [30] for cold-

formed duplex stainless steel sections at elevated temperatures. The material properties of the CFLDSS tubular section at elevated temperatures [26] are presented in Table 5, including Young's modulus (E_T), 0.2% proof stress ($f_{0.2\%,T}$) and ultimate strength ($f_{u,T}$).

The specimen lengths were designed with the same criteria as those for the specimens in the test program [37]. The clear distance of 1.5H was designed for the two adjacent bearing plate edges in EOF loading condition, and for the specimen free end to the adjacent bearing plate edge in ETF and EL conditions. In total, 210 numerical results were generated for the web crippling of CFLDSS tubular sections at elevated temperatures under the loading conditions of EOF, ETF and EL. All these 210 CFLDSS specimens showed pronounced peak loads in the load-deformation curves. Web crippling failure was observed for all specimens except for the specimen series of EOF250×250×12.0N250 and EOF300×200×12.0N200 at elevated temperatures (Table 6). These specimens failed near the mid-span but not at the webs of the specimen ends. Hence, these specimens were not included in the analysis of the present study. The ultimate strengths ($P_{FEA,T}$) of the CFLDSS specimens per web at elevated temperatures are shown in Table 6.

The reduction factors ($P_{FEA,T}/P_{FEA,r}$) of the web crippling strengths for CFLDSS specimens were obtained by normalizing the strengths at elevated temperatures ($P_{FEA,T}$) with that at room temperature ($P_{FEA,r}$) for the same specimen series. The reduction factors ($P_{FEA,T}/P_{FEA,r}$) were compared with those of the material properties of CFLDSS (EN 1.4162) at elevated temperatures, i.e., the factors of E_T/E_r and $f_{0.2,T}/f_{0.2,r}$, as shown in Figures 8-10 for the loading conditions of EOF, ETF and EL, respectively. The E_r and $f_{0.2,r}$ mean the respective Young's modulus and 0.2% proof stress of CFLDSS (EN 1.4162) at room temperature (22 °C in Table 5). The specimens in these figures were distinguished by the web slenderness ratios of h/t. It is shown that CFLDSS tubular sections with higher web slenderness, larger ratios of h/t, maintained residual strengths (larger $P_{FEA,T}/P_{FEA,r}$) better than those with lower web slenderness in the temperatures ranged from 200 to 650 °C, while the residual strengths tended to be similar in the temperatures ranged from 650 to 950 °C, as illustrated in Figures 8-10. The reduction factors of E_T/E_r overestimated the residual strengths of the specimens, while those of $f_{0.2,T}/f_{0.2,r}$ generally underestimated the residual strengths of the specimens in the temperatures ranged from 200 to 650 °C for the three loading conditions. However, both reduction factors of E_T/E_r and $f_{0.2,T}/f_{0.2,r}$ tended to overestimate the residual strengths in the temperatures ranged from 650 to 950 °C for the three loading conditions (Figures 8-10).

6 Reliability analysis

The web crippling design rules in this study were assessed by reliability analysis. The analysis was performed by following the Commentary in the ASCE Specification [3]. However, it should be noted that there are other analysis methods in the specifications, for example, the analyses method in EC0 [45]. Afshan *et al.* [46] proposed statistical data on different types of stainless steel material properties for the reliability analyses specified in EC0 [45]. For the purpose of direct comparison and assessment, the factors and the method in the commentary of the ASCE [3] was used for different predictions in the present study. The reliability index (β) is a relative measure for the design provisions in terms of reliable and probabilistically safe. A target reliability index of 2.5 was set in this study. The design rules are considered to be reliable and probabilistically safe if the β is greater than or equal to 2.5 ($\beta \geq 2.5$). In the calculation of β, the load combination of 1.2DL + 1.6LL was used for the design rules provided by ASCE [3], NAS [39] and Zhou and Young [30], while the combination of 1.35DL + 1.5LL in European code (EC0) [45] was used for the European design rules [5, 47]. The DL represents the dead load and LL represents the live load. The DL/LL was set as 0.2 in ASCE [3]. The suggested mean value and COV of the material factor are M_m = 1.10 and F_m = 1.00, respectively; and those of fabrication factor are V_M = 0.10 and V_F = 0.05 in Section 6.2 of ASCE [3]. In addition, a correction factor (C_P) as specified in ASCE [3] was used to consider the influence of limited test and numerical results. The resistance factor (ϕ) specified in those design rules were used to calculate the corresponding reliability index (β). The reliability analysis of the design rules is discussed in the later sections of this paper.

7 Current design rules and assessments

7.1 General

The current design rules available in most specifications for web crippling of cold-formed steel structures are semi-empirical in nature as the theoretical analysis is quite complex. It should be noted that the web crippling design rules in the current international stainless steel specifications (ASCE [3]; AS/NZS [4] and EN 1993-1-4 [5]) are mainly based on those design specifications for carbon steel. Due to the fundamental difference of stress-strain curves between carbon steel and stainless steel in nature, the applicability of these design rules should be assessed. Furthermore, it should be noted that these design rules may not adequately account for the sections outside the range of variables in the FEA in this study, and they are provided for room temperature condition only, but not for elevated temperature conditions. Nonetheless, the suitability of these design rules (ASCE [3]; AS/NZS [4] and EN 1993-1-4 [5]) was assessed for the predictions of nominal web crippling strengths (unfactored

design strengths) per web of the CFLDSS tubular sections at elevated temperatures subjected to concentrated end bearing loads (EOF, ETF and EL). Apart from the aforementioned stainless steel design specifications, the unified design equation for different loading conditions (including EOF and ETF) specified in the NAS [39] was also used in this study. Note that the unified design equation in NAS [39] is provided for cold-formed carbon steel structural members at room temperature condition. In the calculation of the nominal strengths, the reduced material properties (Table 4) of CFLDSS due to elevated temperatures were used.

The unified design equation in NAS [39] was modified by Zhou and Young [30] by proposing new sets of coefficients. These new coefficients in the unified design equation was proposed for web crippling design of cold-formed duplex stainless steel (EN 1.4462) tubular sections at elevated temperatures under different loading conditions, including EOF and ETF. In the present study, the modified unified design equations was also assessed.

7.2 Design rules

The differences of the design rules in current stainless steel design specifications ASCE [3]; AS/NZS [4] and EN 1993-1-4 [5]) are discussed in detail by Cai and Young [37]. The ASCE Specification [3] and the AS/NZS Standard [4] provide identical design rules. Hence, the design rules in the ASCE [3] were adopted. The web crippling design rules are specified in Section 3.3.4 of the ASCE Specification [3]. The web crippling design rules in the EN 1993-1-4 [5] may refer to those specified in the EN 1993-1-3 [47] for cold-formed steel members, where the design for "Local transverse forces" in Section 6.1.7.3 of the EN 1993-1-3 [47]was used. In addition, the unified design equation (Equation (3-1)) specified in Section G5 of the NAS [39] for web crippling strength cold-formed carbon steel structural members was used.

$$P = Ct^2 f_{0.2} \sin\theta \left(1 - C_R\sqrt{\frac{r}{t}}\right)\left(1 + C_N\sqrt{\frac{N}{t}}\right)\left(1 - C_h\sqrt{\frac{h}{t}}\right) \quad (3\text{-}1)$$

where P = nominal web crippling strength per web, C = overall web crippling coefficient; C_R = inside corner radius coefficient; C_N = bearing length coefficient; C_h = web slenderness coefficient. The coefficients and the application limits specified in NAS [39] for Equation (3-1) are shown in Table 7. In addition, the modified design equation proposed by Zhou and Young [30] for cold-formed duplex stainless steel (EN 1.4462) tubular sections at elevated temperatures are shown in Equation (3-2). The coefficients and the application limits for Equation (3-2) are also presented in Table 7.

$$P = Ct^2 f_{0.2,T} \sin\theta \left(1 - C_R\sqrt{\frac{r}{t}}\right)\left(1 + C_N\sqrt{\frac{N}{t}}\right)\left(1 - C_h\left(\frac{f_{0.2,T}}{E_T}\right)\sqrt{\frac{h}{t}}\right) \quad (3\text{-}2)$$

where $f_{0.2,T}$ and E_T are the yield stress (0.2% proof stress) and the elastic modulus at a given temperature in degree Celsius (°C), respectively.

It should be noted that the loading condition of EL is not provided in the ASCE [3], NAS [39], and Zhou and Young [30]. For the purpose of comparison and assessment, the designs for the loading conditions of EOF and ETF in the ASCE [3], NAS [39] and Zhou and Young [30] were both used for the strength predictions of the EL condition in the present study.

7.3 Assessment of current predictions

The ultimate strengths ($P_{FEA,T}$) per web at elevated temperatures were compared with those predicted by the current design provisions, as shown in Figures 11-13 for the loading conditions of EOF, ETF and EL, respectively. The comparisons were further summarized in Tables 8-10, where in each table, the comparisons were also divided for each temperature level. In the calculation of strength predictions, the material properties in the design equations were substituted by the material properties at elevated temperatures. The material properties (E_T and $f_{0.2,T}$) in Table 4 at elevated temperatures were used as the corresponding stress-strain curves were used for the CFLDSS specimens in the parametric study.

For the CFLDSS specimens subjected to EOF loading condition at elevated temperatures (see Figure 11), the predictions by the ASCE [3] were conservative for all the specimens at room temperature condition (i.e., 22 °C), unconservative for all the specimens in the temperatures ranged from 800 to 950 °C; for the temperatures ranged from 200 to 650 °C, the predictions were unconservative for the stockier webs (e.g., h/t = 21) and conservative for the specimens with web slenderness 40 < h/t < 60. As the web slenderness further increased (e.g., 120 < h/t), the predictions tended to be unconservative, as shown in Figure 11(a). The predictions by EN 1993-1-3 [47] were overall conservative for all the specimens at elevated temperatures (see Figure 11(b)). This is because that the web slenderness ratio (h/t) and the actual bearing lengths (N) are not considered in the design provisions of EN 1993-1-3 [47]. Note that the CFLDSS specimen sections had different web slenderness (h/t) and were loaded by steel plates with different bearing lengths (N). On the contrary to those predictions by the ASCE [3], the predictions by the NAS [39] were unconservative for all the specimens at room temperature condition, but conservative for all the specimens at the temperatures level of 950 °C; for the temperatures ranged from 200 to 800 °C, the predictions were unconservative for the stockier webs (e.g., h/t = 21) and conservative for the specimens with web slenderness of 40 < h/t < 60, as the web slenderness further increased (e.g., 120 < h/t), the predictions became unconservative (see Figure 11(c)). The predictions by Zhou and Young [30] provided similar results as those predicted by NAS [39], however, better predictions were provided for the webs with 40 < h/t < 60 at elevated temperatures, as the ratios of $P_{FEA,T}/P_{Z\&Y}$ were overall closer to 1.0 (see Figure 11(d)).

For the CFLDSS specimens subjected to ETF loading condition at elevated temperatures (see Figure 12), the predictions by the ASCE [3] were conservative for all the specimens at room temperature condition (i.e., 22 °C), generally unconservative for all the specimens in the temperatures ranged from 650 to 950 °C; for the temperatures ranged from 200 to 500 °C, the predictions were generally conservative for the specimens with web slenderness $15 < h/t < 60$. As the web slenderness become larger, $120 < h/t$, the predictions tended to be unconservative (see Figure 12(a)). Similar to those predictions for EOF loading condition, the predictions by EN 1993-1-3 [47] were overall conservative for all the specimens at elevated temperatures (see Figure 12(b)). On the contrary to those predictions by the ASCE [3], the predictions by the NAS [39] were unconservative for all the specimens at room temperature condition, but generally conservative for all the specimens at temperature level of 950 °C; for the temperatures ranged from 200 to 800 °C, the predictions were generally unconservative for all the specimens (see Figure 12(c)). The predictions by Zhou and Young [30] were generally better than those by NAS [39] for the specimens with web slenderness of $15 < h/t < 60$ at elevated temperatures as the ratios of $P_{FEA,T}/P_{Z\&Y}$ were overall closer to 1.0 (see Figure 12(d)).

As mentioned previously, both ETF and EOF design rules were used for the strength predictions of specimens under EL condition by the ASCE [3], NAS [39] and Zhou and Young [30]. The predictions for these provisions [3, 30, 39] by using the design rules for EOF and ETF loading conditions were distinguished by the superscript of "#" and "^", respectively. For the predictions by the ASCE [3], it is shown that the predictions of $P_{ASCE}^{\#}$ were generally conservative for the specimens with web slenderness of $15 < h/t < 60$ in the temperatures ranged from 22 to 350 °C, the predictions for all the specimens tended to be unconservative as when the temperatures exceeded 350 °C, in particular in the temperatures ranged from 650 to 950 °C; while the $P_{ASCE}^{\wedge}$ provided relatively better predictions for all the specimens in the temperatures ranged from 650 to 950 °C as the ratios of $P_{FEA,T}/P_{ASCE}^{\wedge}$ were closer to 1.0, but relatively more conservative predictions for the specimens with web slenderness $15 < h/t < 60$ in the temperatures ranged from 22 to 650 °C (see Figures 13(a)-(b)). Similar to those predictions for EOF and EL conditions, the predictions by EN 1993-1-3 [47] were overall conservative for all the specimens at elevated temperatures (see Figure 13(c)). The predictions of $P_{NAS}^{\#}$ (see Figure 13(d)) and $P_{NAS}^{\wedge}$ (see Figure 13(e)) by NAS [39] were generally unconservative for all the specimens in the temperatures ranged from 22 to 800 °C but generally conservative for the temperature level of 950 °C. For the temperatures ranged from 22 to 800 °C, the predictions by the $P_{NAS}^{\#}$ tended to be more unconservative as the web slenderness h/t increased, while such trend was not found for those by $P_{NAS}^{\wedge}$, instead, the ratios of $P_{FEA,T}/P_{NAS}^{\wedge}$ were generally maintained. The predictions of $P_{Z\&Y}^{\#}$ (see Figure 13(f)) and $P_{Z\&Y}^{\wedge}$ (see Figure 13(g)) by Zhou and Young [30] generally showed similar trend, namely,

as the web slenderness h/t increased, the predictions of $P^{\#}_{Z\&Y}$ and $P^{\wedge}_{Z\&Y}$ tended to be unconservative or more unconservative at elevated temperatures.

The mean value of FEA strength-to-predicted strength with the corresponding COV for each temperature lever and at elevated temperatures (22~950 °C) were illustrated in Tables 8-10 for the loading conditions of EOF, ETF and EL, respectively. For EOF loading condition at elevated temperatures (see Table 8), the mean values for the predictions by ASCE [3] and NAS [39] are 1.01 and 0.99, respectively, with the corresponding COV of 0.333 and 0.253. However, both predictions [3,39] are not reliable with the respective resistance factor (ϕ) due to the values of β smaller than 2.5. The predictions by EN 1993-1-3 [46] are very conservative but reliable, while those predicted by Zhou and Young [30] are unconservative and not reliable. For ETF loading condition at elevated temperatures (see Table 9), the mean value for the predictions by ASCE [3] are a little bit conservative ($P_{FEA,T}/P_{ASCE}$ = 1.04) while those by NAS [39] and Zhou and Young [30] are unconservative, and all these predictions are not reliable with the respective ϕ; however, the predictions by EN 1993-1-3 [47] are conservative and reliable.

For EL condition at elevated temperatures (see Table 10), by using the EOF design rules the predictions by ASCE [3], NAS [39] and Zhou and Young [30], these predictions are unconservative, e.g., $P_{FEA,T}/P^{\#}_{NAS}$ = 0.85 with the COV = 0.281; however, by using the ETF design rules, better predictions were found for NAS [39] and Zhou and Young [30] as the mean values are closer to 1.0 with comparable COVs, e.g., $P_{FEA,T}/P^{\wedge}_{NAS}$ = 0.97 with the COV = 0.243; the predictions by ASCE [3] became conservative, i.e., $P_{FEA,T}/P^{\wedge}_{ASCE}$ = 1.19. It should be noted that all these design rules are not reliable with the respective ϕ due to the values of β were smaller than 2.5, except for the case of $P_{FEA,T}/P^{\wedge}_{ASCE}$. Conservative and reliable predictions by EN 1993-1-3 [47] were found.

8 Proposed design rules and assessments

8.1 General

As discussed in the previous section of this paper, the predictions by the ASCE [3] and NAS [39] were generally unconservative and not reliable for the web crippling of CFLDSS tubular sections at elevated temperatures under the loading conditions of EOF, ETF and EL. The modified unified design equation proposed by Zhou and Young [30] for cold-formed duplex steel at elevated temperatures also provided unconservative and not reliable predictions. Note that the design for the EL condition was not provided in the modified equation [30]. The EN 1993-1-3 [47] provided reliable but conservative (e.g., mean value of $P_{FEA,T}/P_{EC}$ greater than 2.50 for ETF condition) or very

conservative (e.g., mean value of $P_{FEA,T}/P_{EC}$ greater than 3.50 for EOF condition) predictions. Hence, new design method is proposed for the web crippling design of CFLDSS tubular sections at elevated temperatures, under the loading conditions of EOF, ETF and EL in this study.

The Direct Strength Method (DSM) [48] is an alternative way to determine the strength of cold-formed steel members. It provides strength predictions by avoiding the calculation of effective areas for steel members in the design, for example, steel columns subjected to axial loading. Hence, the DSM could be more convenient than the conventional design method when the effective area of a slender section is not easy to find out. The DSM has been developed for the design of cold-formed steel beams and columns, and is documented in the design specifications, such as the NAS [39]. It should be noted that the current DSM in design specifications does not provide design rules for web crippling design of cold-formed steel members. Investigations of DSM for the web crippling design of cold-formed steel members under different loading conditions have been conducted by researchers in the last few years, such as Duarte and Silvestre [49], Keerthan *et al*. [50], Natário *et a*l. [51,52] and Heurkens *et al*. [53] for cold-formed steel open sections, Bock and Real [54] for cold-formed ferritic and austenitic stainless steel hat sections, Li and Young [32,33] for cold-formed ferritic stainless steel rectangular and square hollow sections. A more recent study by Cai and Young [55] extended the DSM for the web crippling design of CFLDSS tubular sections under the loading conditions of EOF, ETF and EL. However, these DSM methods [32-33, 49-55] for web crippling design were proposed for the design at room temperature condition, but not for elevated temperature conditions. In this study, efforts on the modifications of DSM are made to extend its application for web crippling design of CFLDSS tubular sections at elevated temperatures.

8.2 Modified DSM

The format of DSM presented in Li and Young [32] and Cai and Young [55] for web crippling design of stainless steel sections at room temperature is illustrated in Equation (4), where different sets of coefficient for a, b, n, γ and λ_k in Equation (4) were proposed depends on stainless steel grades and loading conditions. There are two different types of web crippling failure for cold-formed stainless steel square and rectangular hollow sections. They are web buckling, where the web crippling capacity mainly depends on the stiffness of the material, and yielding in the section, where the web crippling capacity mainly depends on the yield strength of the material [30]. As presented in Figures 8-10, the reduction factors of the web crippling strength ($P_{FEA,T}/P_{FEA,r}$), 0.2% proof stress ($f_{0.2,T}/f_{0.2,r}$) and Young's modulus (E_T/E_r) of CFLDSS sections generally showed the similar reduction trends at elevated temperature for different loading conditions. Hence, in this study, the factor χ to consider the effects of 0.2% proof stress ($f_{0.2,T}$) and Young's modulus (E_T) of the material properties at elevated temperatures was proposed, as shown in Equation (5). The CFLDSS tubular sections subjected to web

463 crippling ($P_{DSM,T}$) at elevated temperatures could then be calculated by χP_{DSM}, as illustrated in Equation
464 (6).

465 $$P_{DSM} = \begin{cases} \gamma P_{y,T} & \lambda \le \lambda_k \\ a\left[1 - b\left(\frac{P_{cr,T}}{P_{y,T}}\right)^n\right]\left(\frac{P_{cr,T}}{P_{y,T}}\right)^n P_{y,T} & \lambda > \lambda_k \end{cases} \quad (4)$$

466 $$\chi = \frac{1}{0.0036}\left(\frac{f_{0.2,T}}{E_T}\right) \quad (5)$$

467 $$P_{DSM,T} = \chi P_{DSM} \quad (6)$$

468 where $\lambda = \sqrt{P_{y,T}/P_{cr,T}}$ is the web crippling slenderness ratio. The $P_{cr,T}$ and $P_{y,T}$ are the nominal
469 bearing strengths per web for buckling and yielding at elevated temperatures, respectively.

470 The DSM generally requires aid from computer software to compute the nominal bearing
471 strength for buckling at room temperature, e.g., the DSM proposed by Natário *et al*. [51,52]. However,
472 this is not a necessary for the calculation of $P_{cr,T}$ in Equation (4). Instead, the calculations of $P_{cr,T}$ and
473 $P_{y,T}$ could be done manually by referring Clause 5.13 of the AS 4100 [56], as suggested and adopted
474 by Li and Young [32,33] for room temperature condition, and depicted in the following Equations (7)-
475 (11). It should be noted that these equations are provided for the design at room temperature condition
476 [52], but not for elevated temperature conditions. Hence, in these calculations, the 0.2% proof stress
477 ($f_{0.2,r}$) at room temperature was replaced by those ($f_{0.2,T}$) at elevated temperatures.

478 $$P_{cr,T} = \alpha_c t N_m f_{0.2,T} \quad (7)$$

479 where α_c is the slenderness reduction factor as specified in Clause 6.3.3 of the AS 4100 [56], N_m is the
480 mechanism length for the loading conditions of EOF, ETF and EL, which could be determined by the
481 following Equation (8):

482 $$N_m = N + 2.5R + 0.5h \quad (8)$$

483 where R is the outer corner radius.

484 $$P_{y,T} = \alpha_p t N_m f_{0.2,T} \quad (9)$$

485 For EOF, ETF and EL conditions:

486 $$\alpha_p = \sqrt{2 + k_s^2} - k_s \quad (10)$$

487 where $k_s = 2R/t$-1.

488 Similar to those suggested by Li and Young [32,33] and by Cai and Young [55], different
489 values of a, λ_k and γ are proposed for different loading conditions. However, the constant coefficients
490 of b = 0.20 and n = 0.60 as well as resistance factor of ϕ = 0.80 are proposed regardless of different

loading conditions. These coefficients (see Table 11) are proposed for the web crippling design at elevated temperature conditions, and applicable for CFLDSS square and rectangular hollow sections having stiffened or partially stiffened flanges with the limits for $10 \leq h/t \leq 145$, $r/t \leq 2.0$, $N/t \leq 150$ and $N/h \leq 1.5$. The coefficients for the Equation (4) were calibrated against the 196 numerical results (Table 6) at elevated temperatures in this study. Furthermore, the coefficients for the Equation (4) were also calibrated against the 47 test results [37] of CFLDSS sections at room temperature under the loading conditions of EOF, ETF and EL.

8.3 Assessment of modified DSM predictions

The ultimate strengths ($P_{FEA,T}$) per web at elevated temperatures were compared with those predicted by the modified DSM ($P_{DSM,T}$) using the newly proposed coefficients (Table 11), as shown in Figures 14(a)-(c) for the loading conditions of EOF, ETF and EL, respectively. The comparisons were also summarized in Tables 8-10, as those comparisons for the current predictions presented in Section 7.3.

It is shown that the modified DSM ($P_{DSM,T}$) generally provided conservative predictions for the web crippling strengths of CFLDSS tubular sections at elevated temperature. However, unlike those predictions by Zhou and Young [30] (see Figures 11(d), 12(d) and 14(g)) and some other predictions that showed the reduction trends with the increment of h/t at each temperature level, the effects of h/t on the predictions by the modified DSM at each temperature level were to some extent eliminated, except for those at the temperature level of 950 °C. As shown in Tables 8-10, the predictions by the modified DSM ($P_{DSM,T}$) are conservative at each temperature level for the three loading conditions, except for those at room temperature (22 °C) for the ETF loading condition, $P_{FEA,T}/P_{DSM,T} = 0.91$. The overall conservative predictions for each loading conditions are mainly due to the very conservative predictions for the strengths at the temperature levels of 650 and 950 °C, as shown in the mean values of $P_{FEA,T}/P_{DSM,T}$ (see Tables 8-10). These data are further illustrated in Figures 15-17. The comparisons of the numerical results at elevated temperatures with the DSM curves (using Equation (4)) for the loading conditions of EOF, ETF and EL are shown in Figures 15-17, respectively. In each figure, the ratio of $(1/\chi)(P_{FEA,T}/P_{y,T})$ were plotted against the web crippling slenderness ratio of $(P_{y,T}/P_{cr,T})^{0.5}$.

Reliability analysis were also conducted for the ultimate strength ($P_{DSM,T}$) predicted by using the modified DSM are reliable for all the three loading conditions at elevated temperatures. The aforementioned values for the material factor and fabrication factor in Section 6 were adopted. In addition, the load combination of 1.2DL + 1.6LL was used. The reliability indices (β) were computed based on the resistance factor of 0.80 ($\phi = 0.80$ see Table 12). It is shown that the predictions by the modified DSM are reliable as evidenced by the values of reliability indices greater than the target value of 2.5 ($\beta > 2.5$).

The web crippling strengths (P_t) of CFLDSS square and rectangular hollow sections at room temperature (22 °C) from the 47 tests conducted by Cai and Young [37] were also used to compared with the strengths ($P_{DSM,T}$) predicted by using the proposed DSM equation, Equation (6), for elevated temperature conditions, as shown in Tables 12-14. The same values of the coefficients in Table 11 for CFLDSS tubular sections at elevated temperatures were used in the calculation. The same factors and load combination used for the reliability analysis in the previous paragraph were adopted. It is shown that the predicted strengths are overall conservative and reliable for the three loading conditions (EOF, ETF and EL), as reflected by the mean values of $P_t/P_{DSM,T}$ greater than 1.00 with their corresponding reliability indices (β) greater than 2.5.

9 Conclusions

Non-linear finite element models (FEMs) were developed for the web crippling of cold-formed lean duplex stainless steel (CFLDSS) square and rectangular hollow sections under concentrated end bearing loads, namely, the loading conditions of End-One-Flange (EOF), End-Two-Flange (ETF) and End Loading (EL). After successful verification of the FEMs against with the 36 test results, an extensive parametric study of 210 CFLDSS tubular sections at elevated temperatures was performed. These sections were subjected to web crippling under the three concentrated end bearing loads at different temperatures ranged from 22 (room temperature) to 950 °C. The CFLDSS specimens were carefully designed to cover a wide range of the key parameters, including the ratios of flat web height (h) to thickness (t) with h/t ranged from 21.0 to 145.0, bearing length (N) to web thickness (t) with N/t ranged from 8.3 to 125.0, as well as the ratio of N/h ranged from 0.36 to 1.24.

The appropriateness of the web crippling design rules in the current international specifications (ASCE [3], AS/NZS [4], NAS [39] and EN 1993-1-3 [47]) has been examined by comparing their ultimate strength predictions with those obtained from the finite element analysis for CFLDSS at elevated temperatures. In these codified calculations, the material properties at room (ambient) temperature condition were substituted by those at elevated temperatures. Furthermore, the modified unified design equation [30] in the literature for web crippling of cold-formed duplex stainless steel at elevated temperatures was also assessed. The reliability of the design provisions was assessed by reliability analysis. It was found that the predictions by the ASCE, AS/NZS, NAS and the modified unified design equation were generally unconservative and not reliable for the web crippling of CFLDSS tubular sections at elevated temperatures under the loading conditions of EOF, ETF and EL. The EN 1993-1-3 [47] provided reliable but generally very conservative predictions.

A new design method is then proposed in this study, by considering the effects of 0.2% proof stress and Young's modulus at elevated temperatures and by proposing new sets of coefficients for the Direct Strength Method (DSM) under the loading conditions of EOF, ETF and EL. The proposed design method was calibrated against the numerical results obtained from parametric study and tests. It is shown that the predictions by using the new method are generally conservative and reliable for CFLDSS square and rectangular hollow sections at elevated temperatures under the three loading conditions. Therefore, the newly proposed method is applicable for web crippling (loading conditions of EOF, ETF and EL) design of CFLDSS square and rectangular hollow sections at elevated temperatures with limits of $21 \leq h/t \leq 145$, $r_i/t \leq 2.0$, $N/t \leq 125$ and $N/h \leq 1.25$. The flanges of the CFLDSS tubular sections are stiffened or partially stiffened that unfastened to the supports.

References

[1] Ronald, L.P., Clara, H., Doris, M.E., Paulo, R.R., Angelo, F.P. A Short Review on Wrought Austenitic Stainless Steels at High Temperatures: Processing, Microstructure, Properties and Performance. Materials Research 2007; 10 (4): 453-460.

[2] Gardner, L. Stability and design of stainless steel structures – Review and outlook, Thin-Walled Structures 2019; 141: 208-216.

[3] ASCE. Specification for the design of cold-formed stainless steel structural members. American Society of Civil Engineers (ASCE), ASCE Standard, SEI/ASCE-8-02, Reston, Virginia, 2002.

[4] AS/NZS. Cold-formed stainless steel structures. AS/NZS 4673:2001, Australian/New Zealand Standard (AS/NZS), Standards Australia, Sydney, Australia, 2001.

[5] Eurocode 3. Design of steel structures - Part 1.4: General rules - Supplementary rules for stainless steels. EN 1993-1-4:2006+A1:2015, Brussels, Belgium, European Committee for Standardization, 2015.

[6] Huang, Y., Young, B. Material properties of cold-formed lean duplex stainless steel sections. Thin-Walled Structures 2012; 54: 72-81.

[7] Saliba, N., Gardner, L. Cross-section stability of lean duplex stainless steel welded I-sections. Journal of Constructional Steel Research 2013; 18: 1-14.

[8] Huang, Y., Young, B. Experimental and numerical investigation of cold-formed lean duplex stainless steel flexural members. Thin-Walled Structures 2014; 73: 216-228.

[9] Huang, Y., Young, B. Tests of pin-ended cold-formed lean duplex stainless steel columns. Journal of Constructional Steel Research 2013; 82: 203-215.

[10] Zhao, O., Rossi, B., Gardner, L., Young, B. Behaviour of structural stainless steel cross-sections under combined loading - Part I: Experimental study. Engineering Structures 2015; 89: 236-246.

[11] Zhao, O., Rossi, B., Gardner, L., Young, B. Behaviour of structural stainless steel cross-sections under combined loading - Part II: Numerical modelling and design." Engineering Structures 2015; 89: 247-259.
[12] Saliba, N., Gardner, L. Experimental study of the shear response of lean duplex stainless steel plate girders. Engineering Structures 2013; 46: 375-391.
[13] Saliba N., Real, E., Gardner, L. Shear design recommendations for stainless steel plate girders." Engineering Structures 2014; 59: 220-228.
[14] Cai, Y., Young, B. Structural behavior of cold-formed stainless steel bolted connections. Thin-Walled Structures 2014; 83: 147-156.
[15] Design of steel structures—Part 1.4: general rules— supplementary rules for stainless steels. EN 1993-1-4. Brussels: European Committee for Standardization; 2006.
[16] Feng, M., Wang, Y.C., Davies, J.M. Structural behaviour of cold-formed thin-walled short steel channel columns at elevated temperatures - Part 1: experiments. Thin-Walled Structures 2003; 41 (6): 543-570.
[17] Feng, M., Wang, Y.C., Davies, J.M. Structural behaviour of cold-formed thin-walled short steel channel columns at elevated temperatures - Part 2: design calculations and numerical analysis. Thin-Walled Structures 2003; 41 (6): 571-594.
[18] Chen, J., Young, B. Design of high strength steel columns at elevated temperatures, Journal of Constructional Steel Research 2008; 64 (6): 689-703.
[19] Ranawaka1, T., Mahendran, M. Numerical modelling of light gauge cold-formed steel compression members subjected to distortional buckling at elevated temperatures. Thin-Walled Structures 2010; 48: 334-344.
[20] Cheng, S., Li, L.-Y., Kim, B. Buckling analysis of cold-formed steel channel-section beams at elevated temperatures. Journal of Constructional Steel Research 2015; 104: 74-80.
[21] Landesmanna, A., Camotim, D. Distortional failure and DSM design of cold-formed steel lipped channel beams under elevated temperatures. Thin-Walled Structures 2016; 98: 75-93.
[22] Li, H.-T., Young, B. Cold-formed high strength steel SHS and RHS beams at elevated temperatures. Journal of Constructional Steel Research 2019; 158: 475-485.
[23] Gardner, L., Insaustia, A., Ng, K.T., Ashraf, M. Elevated temperature material properties of stainless steel alloys. Journal of Constructional Steel Research 2010; 66 (5): 634-647
[24] Chen, J., Jin, W.-L. Behaviour of cold-formed stainless steel beams at elevated temperatures. Journal of Zhejiang University-SCIENCE A 2008; 9: 1507-1513.
[25] Feng, R., Young, B. Design of cold-formed stainless steel tubular joints at elevated temperatures. Engineering Structures 2012; 35: 188-202
[26] Cai, Y., Young, B. Behavior of cold-formed stainless steel single shear bolted connections at elevated temperatures. Thin-Walled Structures 2014; 75: 63-75.
[27] Cai, Y., Young, B. Transient state tests of cold-formed stainless steel single shear bolted connections. Engineering Structures 2014; 81: 1-9.
[28] Cai, Y., Young, B. High temperature tests of cold-formed stainless steel double shear bolted connections. Journal of Constructional Steel Research 2015, 104: 49-63.
[29] Cai, Y., Young, B. Bearing resistance design of stainless steel bolted connections at ambient and elevated temperatures. Steel and Composite Structures 2018, 29(2): 273-286.
[30] Zhou, F., Young, B. Web crippling behaviour of cold-formed duplex stainless steel tubular sections at elevated temperatures. Engineering Structures 2013; 57: 51-62.

[31] Zhou, F., Young, B. Cold-formed high-strength stainless steel tubular sections subjected to web crippling. Journal of Structural Engineering 2007; 133(3): 368-377.
[32] Li, H-T., Young, B. Cold-formed ferritic stainless steel tubular structural members subjected to concentrated bearing loads. Engineering Structures 2017; 145: 392-405.
[33] Li, H-T., Young, B. Web crippling of cold-formed ferritic stainless steel square and rectangular hollow sections. Engineering Structures 2018; 176: 968-980.
[34] Bock, M., Arrayago, I., Real, E., Mirambell, E. Study of web crippling in ferritic stainless steel cold formed sections. Thin-Walled Structures 2013, 69: 29-44.
[35] dos Santos, G.B., Gardner L., Kucukler M. Experimental and numerical study of stainless steel I-sections under concentrated internal one-flange and internal two-flange loading. Engineering Structures 2018; 175: 355-370.
[36] dos Santos, G.B., Gardner L. Testing and numerical analysis of stainless steel I-sections under concentrated end-one-flange loading. Journal of Constructional Steel Research 2019; 157: 271-281.
[37] Cai, Y., Young, B. Web crippling of lean duplex stainless steel tubular sections under concentrated end bearing loads. Thin-Walled Structures 2019; 134: 29-39.
[38] Cai, Y., Young, B. Cold-formed lean duplex stainless steel tubular members under concentrated interior bearing loads. Journal of Structural Engineering 2019; ASCE. 145(7): 04019056.
[39] North American Specification (NAS) North American Specification for the design of cold-formed steel structural members. AISI S100–16, Washington D. C., USA: American Iron and Steel Institute (AISI); 2016.
[40] Zhou, F., Young, B. Web crippling of cold-formed stainless steel tubular sections. Advances in Structural engineering 2008; 11(6): 679-691.
[41] ABAQUS. Analysis User's Manual, ABAQUS, Inc., Version 6.20, 2019.
[42] Lian, Y., Uzzaman, A., Lim, J.B.P., Abdelal, G., Nash, D., Young, B. Effect of web holes on web crippling strength of cold-formed steel channel sections under end-one-flange loading condition - Part I: Tests and finite element analysis. Thin-Walled Structures 2016; 107: 443-452
[43] Gardner, L., Nethercot, D.A. Experiments on stainless steel hollow sections—Part 1: Material and cross-sectional behavior. Journal of Constructional Steel Research 2004; 60(9): 1291-1318.
[44] Ala-Outinen T. Fire resistance of austenitic stainless steels Polarit 725 (EN 1.4301) and Polarit 761 (EN 1.4571). VTT Research Notes 1760. Espoo, Finland, 1996.
[45] Afshan, S., Francis, P., Baddoo, N.R., Gardner, L. Reliability analysis of structural stainless steel design provisions. Journal of Constructional Steel Research 2015; 114: 293-304.
[46] EC0. Eurocode 0: basis of structural design. EN 1990:2002+A1:2005. Brussels, Belgium: European committee for standardization; 2005.
[47] Eurocode 3: Design of steel structures - Part 1-3: General rules - Supplementary rules for cold-formed members and sheeting. EN 1993-1-3, Brussels, Belgium: European committee for standardization; 2006.
[48] Schafer, B.W. Review: The Direct Strength Method of cold-formed steel member design. Journal of Constructional Steel Research 2008; 64(7-8): 766-778.
[49] Duarte, A.P.C., Silvestre, N. A new slenderness-based approach for the web crippling design of plain channel steel beams International. Journal of Steel Structures 2013; 13: 421-434.
[50] Keerthan, P., Mahendran, M., Steau, E. Experimental study of web crippling behaviour of hollow flange channel beams under two flange load cases. Thin-Walled Structure 2014; 85:207-19.
[51] Natário, P., Silvestre, N., Camotim, D. Direct strength prediction of web crippling failure of beams under ETF loading. Thin-Walled Structures 2016; 2(98): 360-74.

[52] Natário, P., Silvestre, N., Camotim, D. Web crippling of beams under ITF loading: a novel DSM-based design approach. Journal of Constructional Steel Research 2017; 128: 812-24.
[53] Heurkens, R.A.J., Hofmeyer, H., Mahendran, M., Snijder, H.H. Direct strength method for web crippling - lipped channels under EOF and IOF loading. Thin-Walled Structures 2018; 123: 126-141.
[54] Bock, M., Real, E. Strength curves for web crippling design of cold-formed stainless steel hat sections. Thin-Walled Structures 2014; 85: 93-105.
[55] Cai, Y., Young, B. Design of lean duplex stainless steel tubular sections subjected to concentrated end bearing loads. Journal of Structural Engineering 2020; ASCE, In publication.
[56] Australian Standard (AS). Steel structures. AS 4100, Sydney, Australia: Standards Australia; 1998.

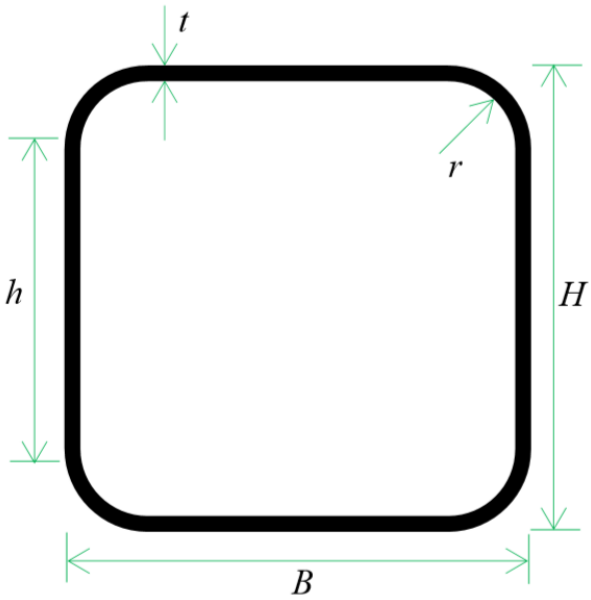

Figure 1: Definition of symbols in a tubular section

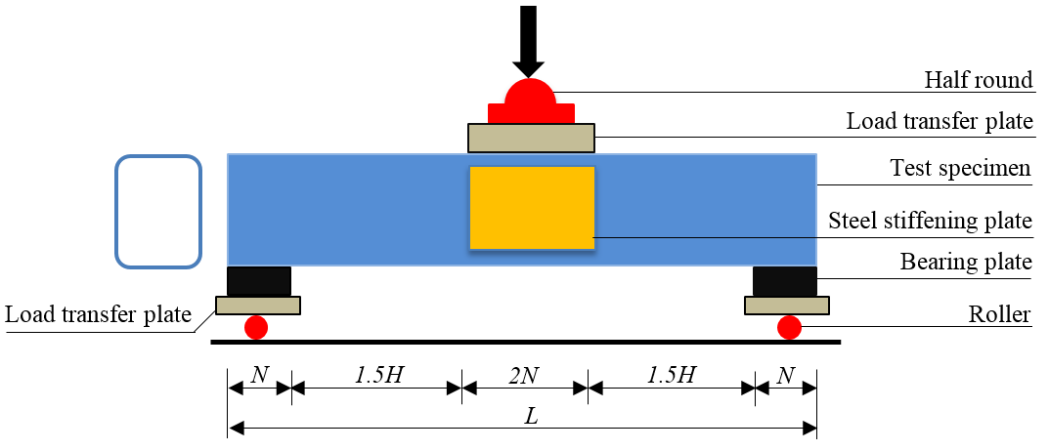

(a) End-One-Flange (EOF) loading condition

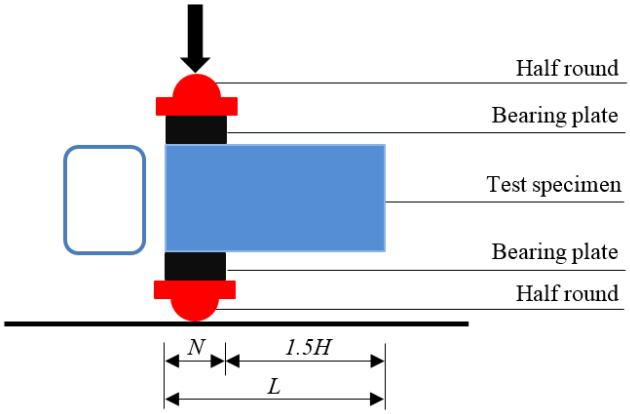

(b) End-Two-Flange (ETF) loading condition

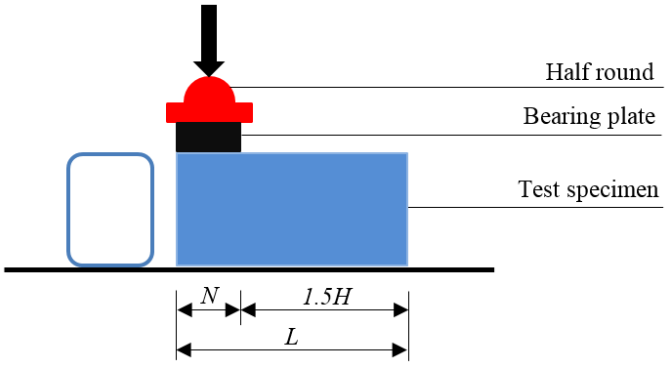

(c) End loading (EL) condition

Figure 2: LDSS specimens under different concentrated end bearing loads [37]

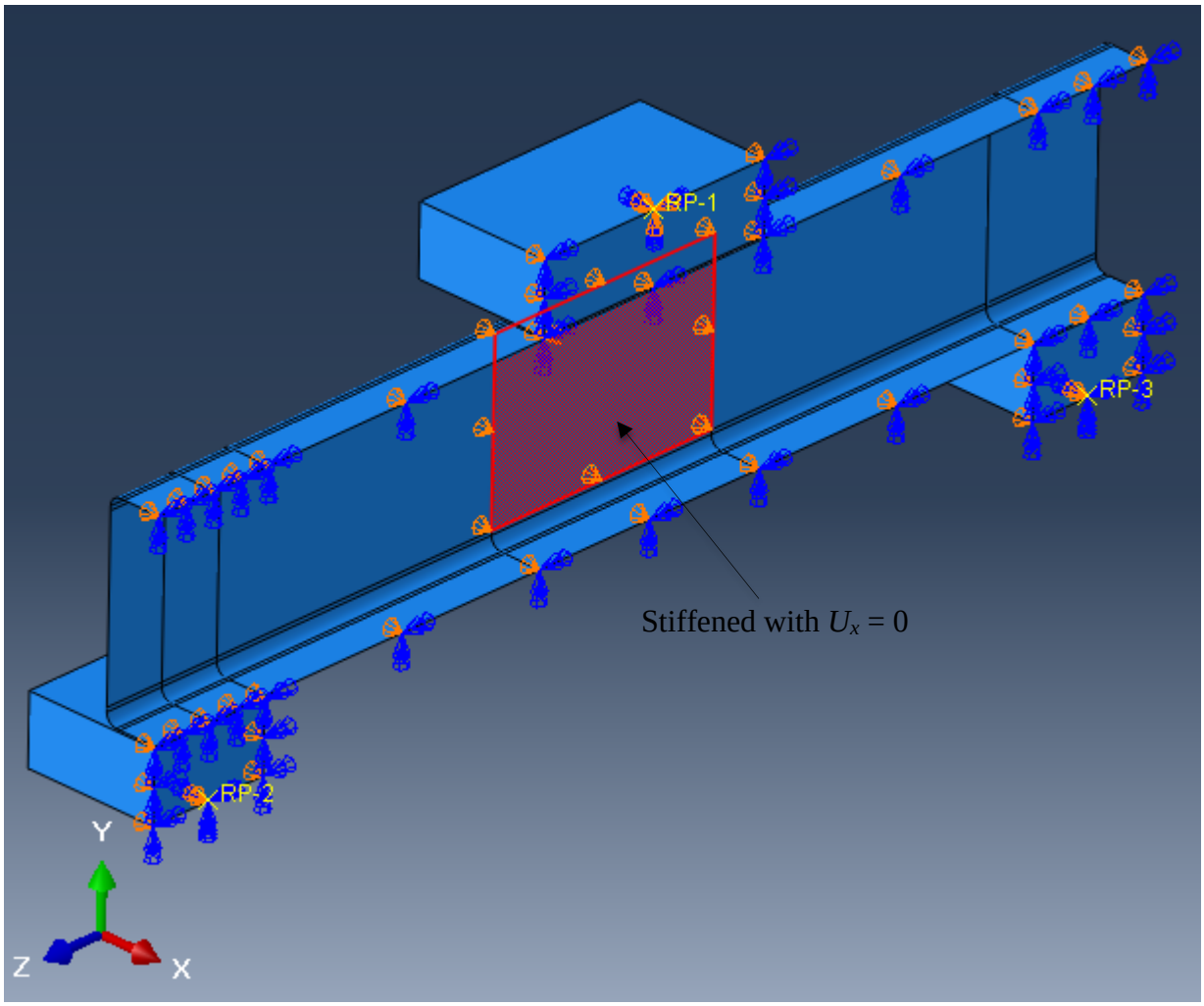

Figure 3: Symmetric finite element model (FEM) for specimen under EOF loading condition

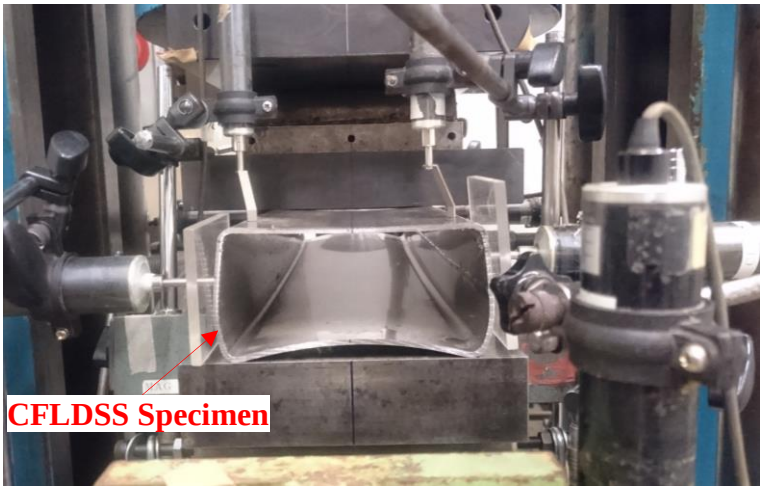

(a) Web crippling test

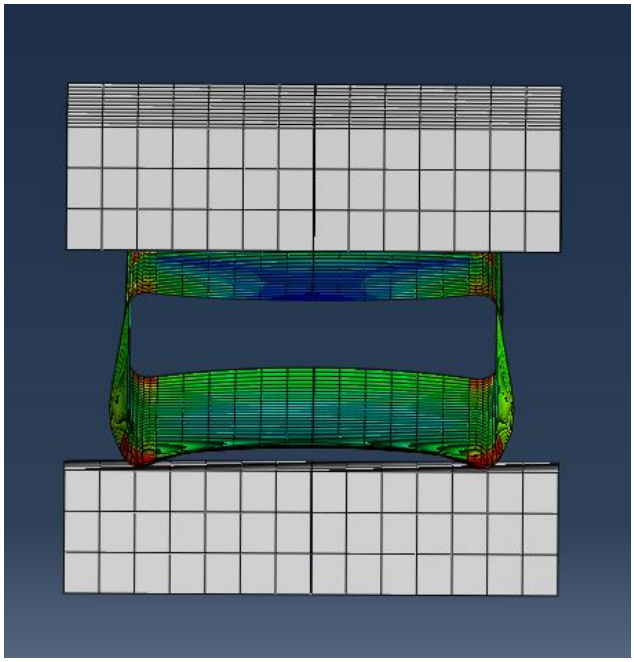

(b) Model of finite element analysis

Figure 4: Comparison of test and numerical failure modes for Specimen EOF80×150×3.0N90

(a) Web crippling test

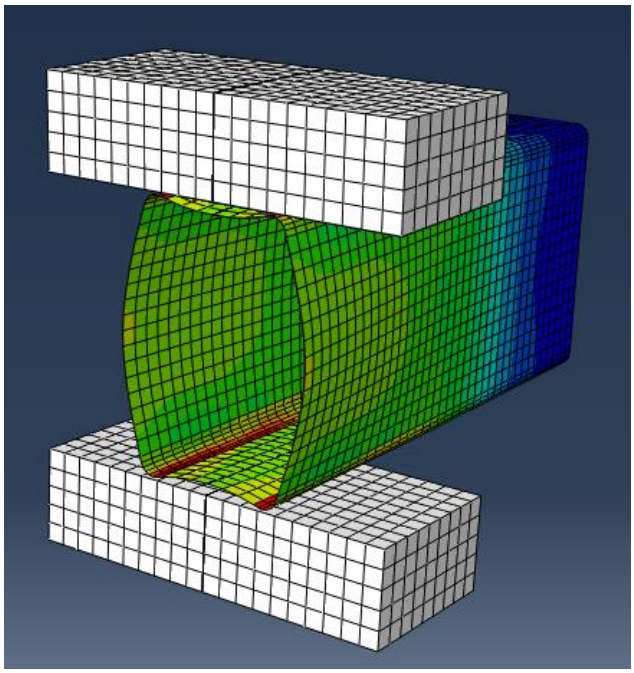

(b) Model of finite element analysis

Figure 5: Comparison of test and numerical failure modes for Specimen ETF150×80×3.0N90

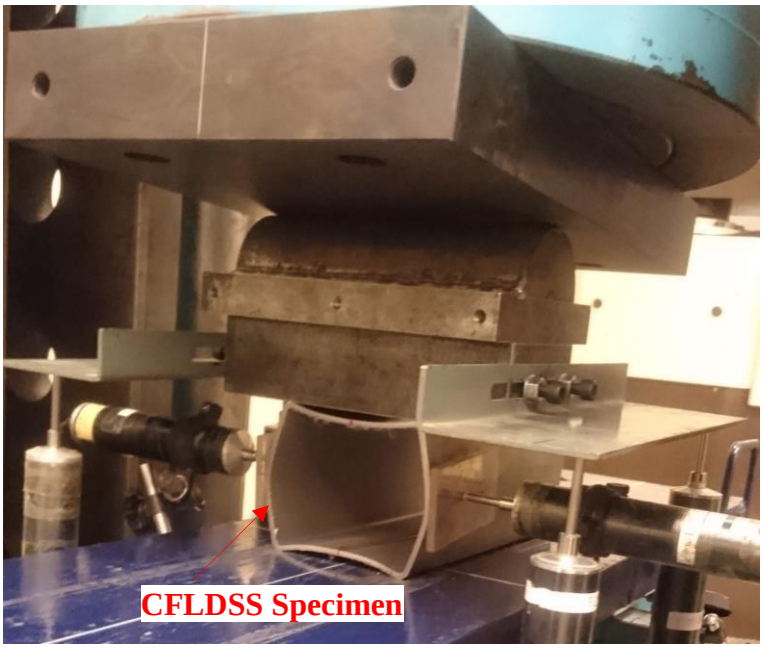

(a) Web crippling test

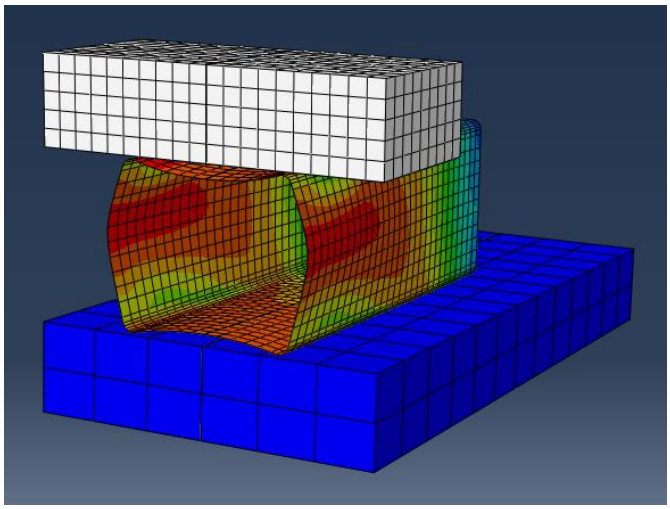

(b) Model of finite element analysis

Figure 6: Comparison of test and numerical failure modes for Specimen EL100×100×3.0N90

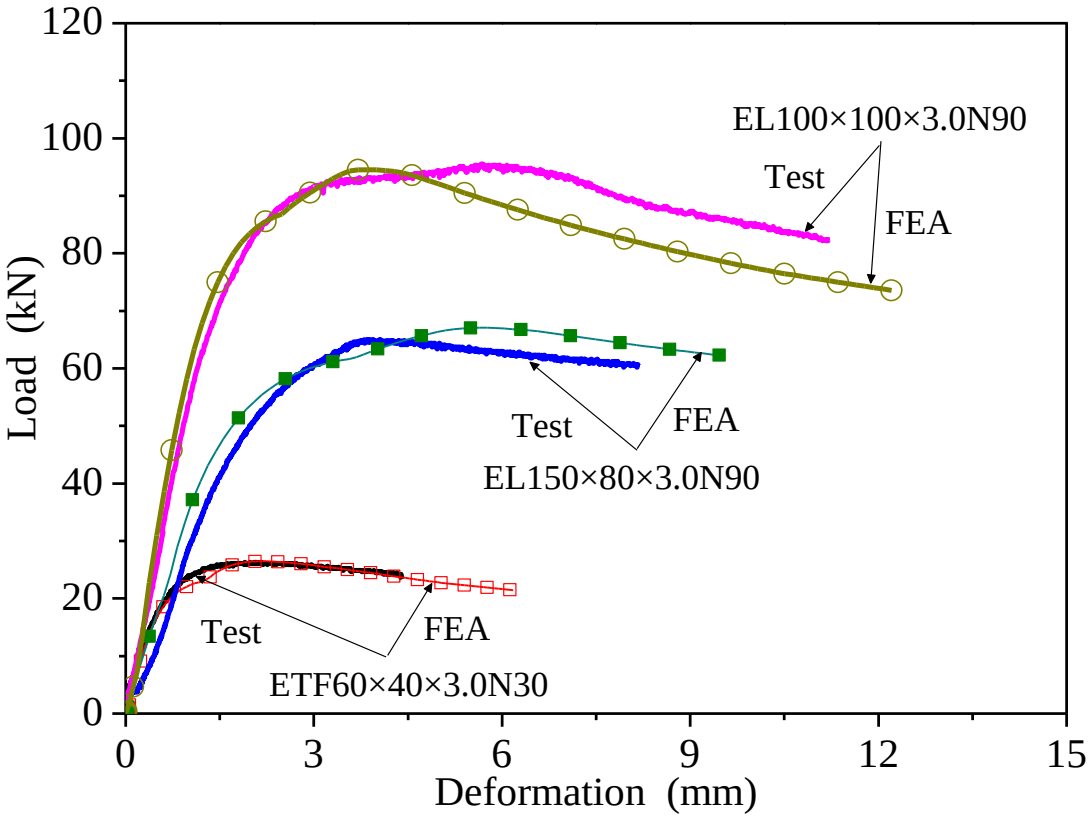

Figure 7: Comparison of load-deformation curves obtained from tests and FEA

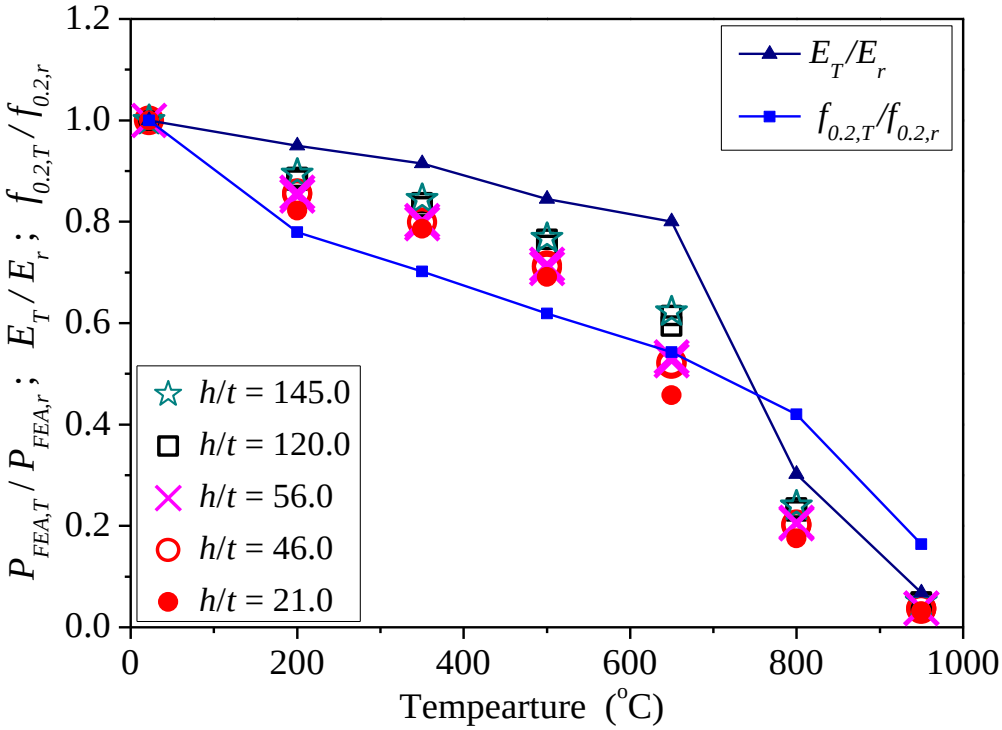

Figure 8: Comparison of reduction factors for EOF loading condition

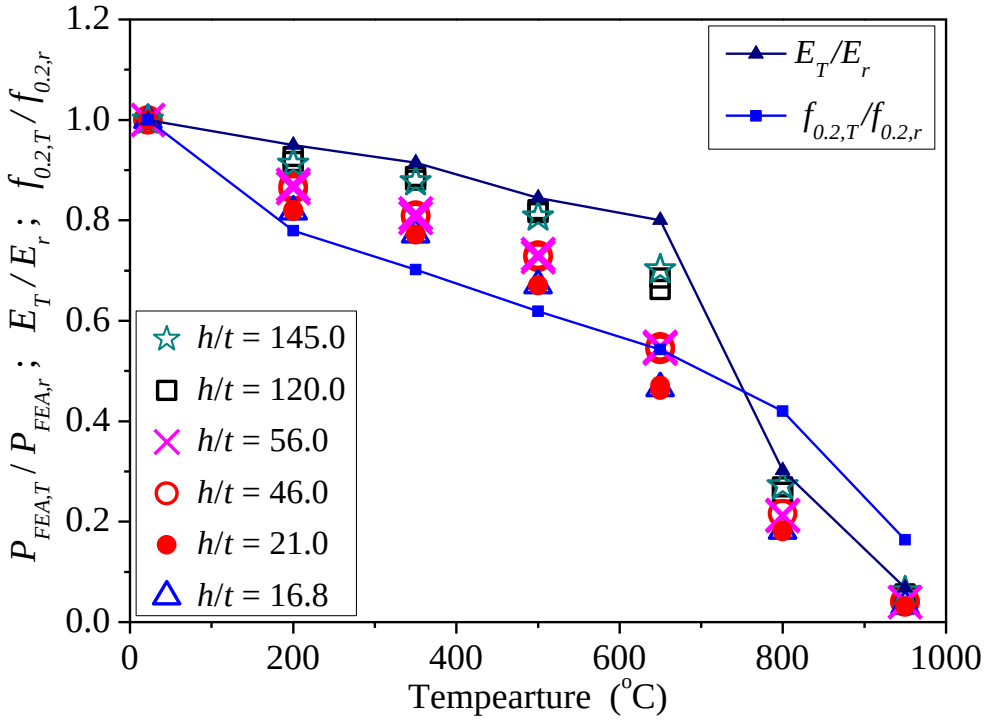

Figure 9: Comparison of reduction factors for ETF loading condition

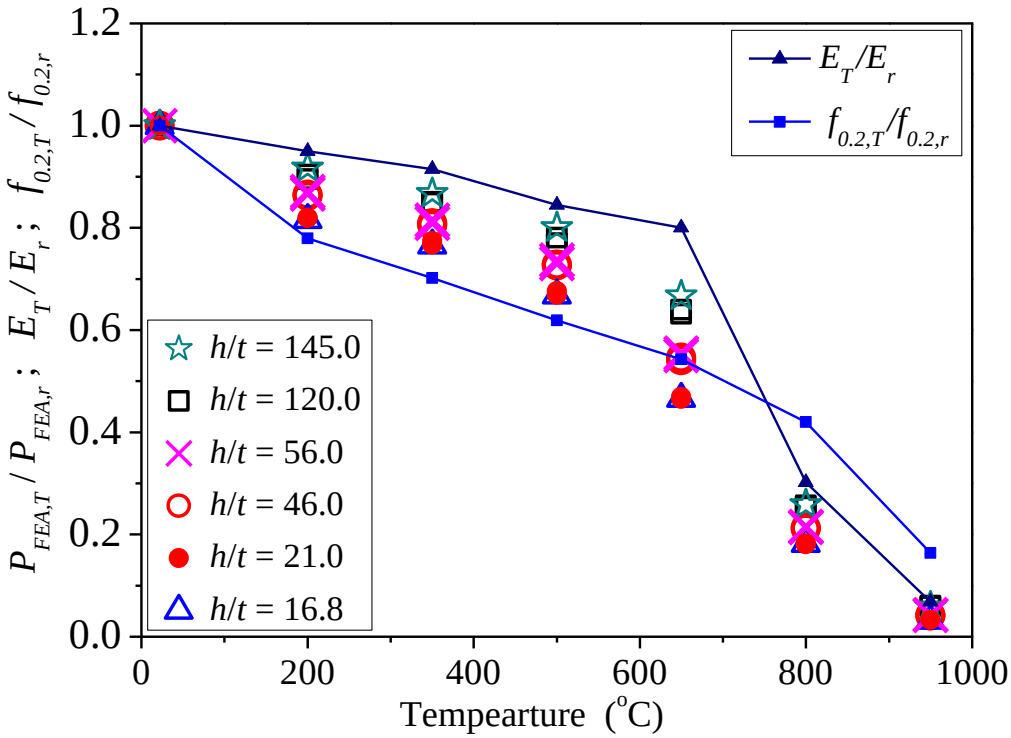

Figure 10: Comparison of reduction factors for EL condition

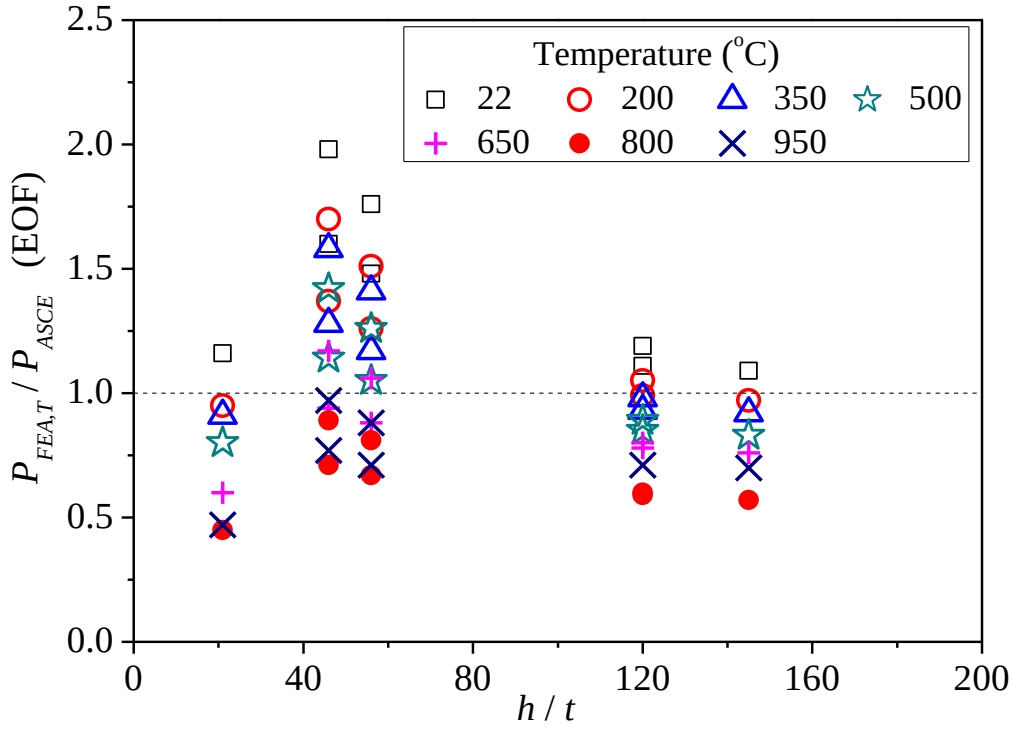

(a) ASCE [3] for EOF

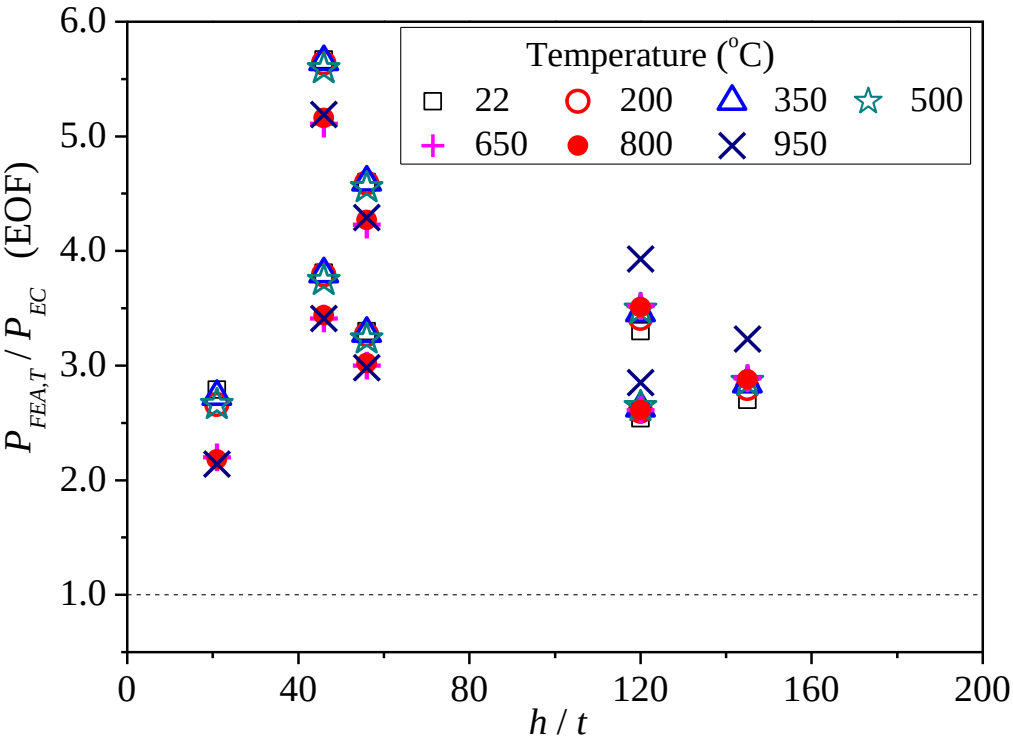

(b) EN 1993-1-3 [47] for EOF

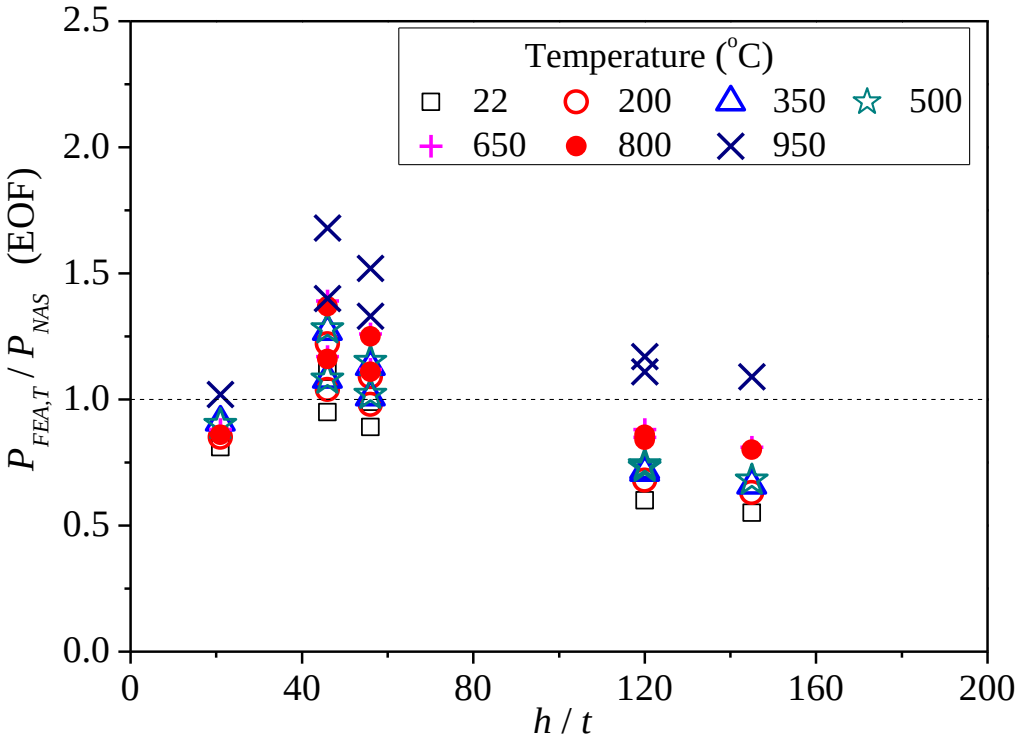

(c) NAS [39] for EOF

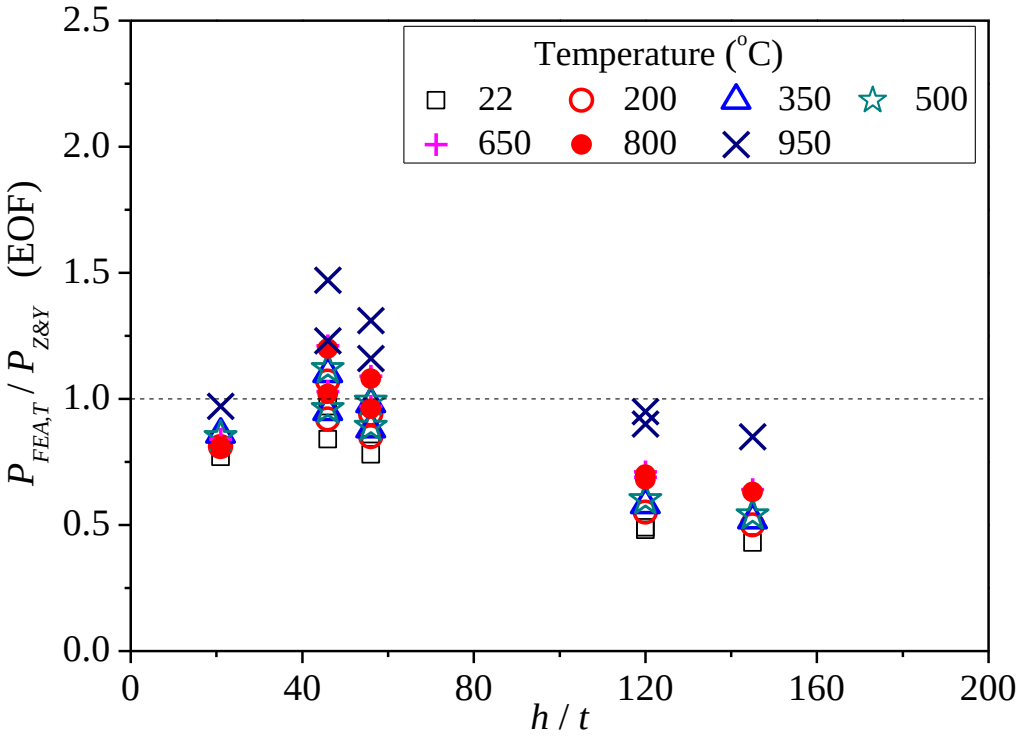

(d) Zhou and Young [30] for EOF

Figure 11: Comparison of FE results with current predictions for EOF loading condition

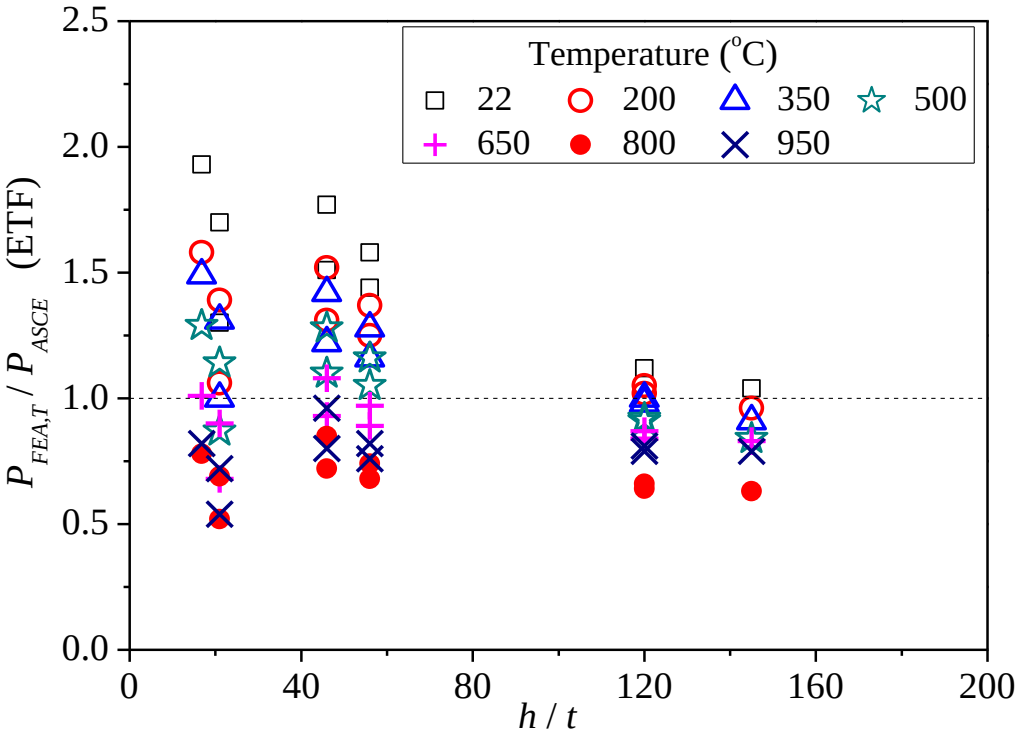

(a) ASCE [3] for ETF

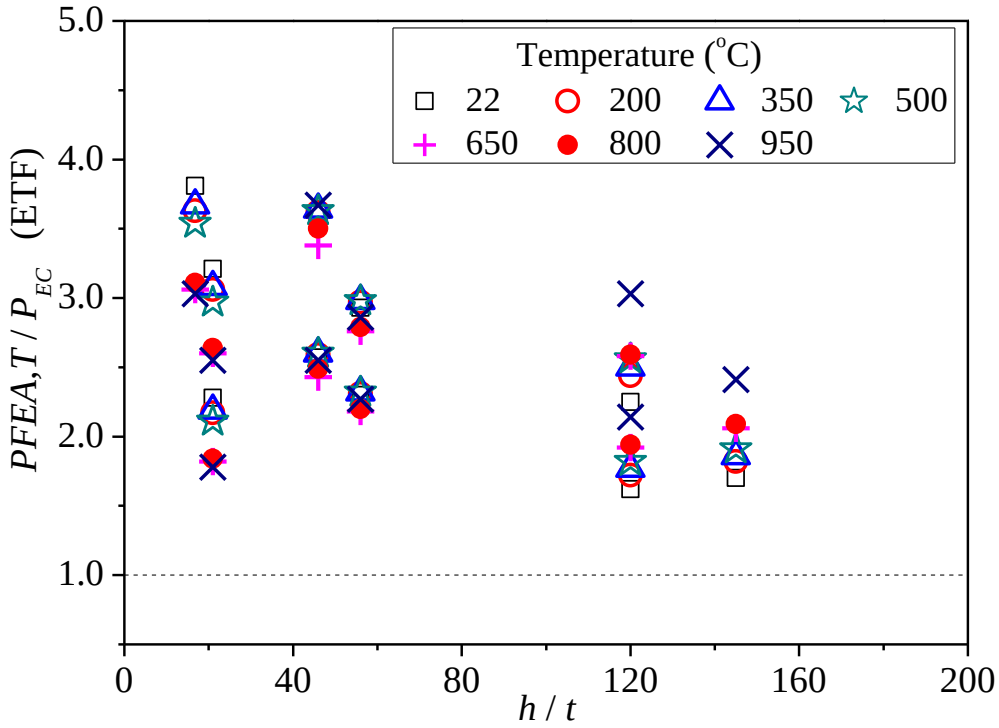

(b) EN 1993-1-3 [47] for ETF

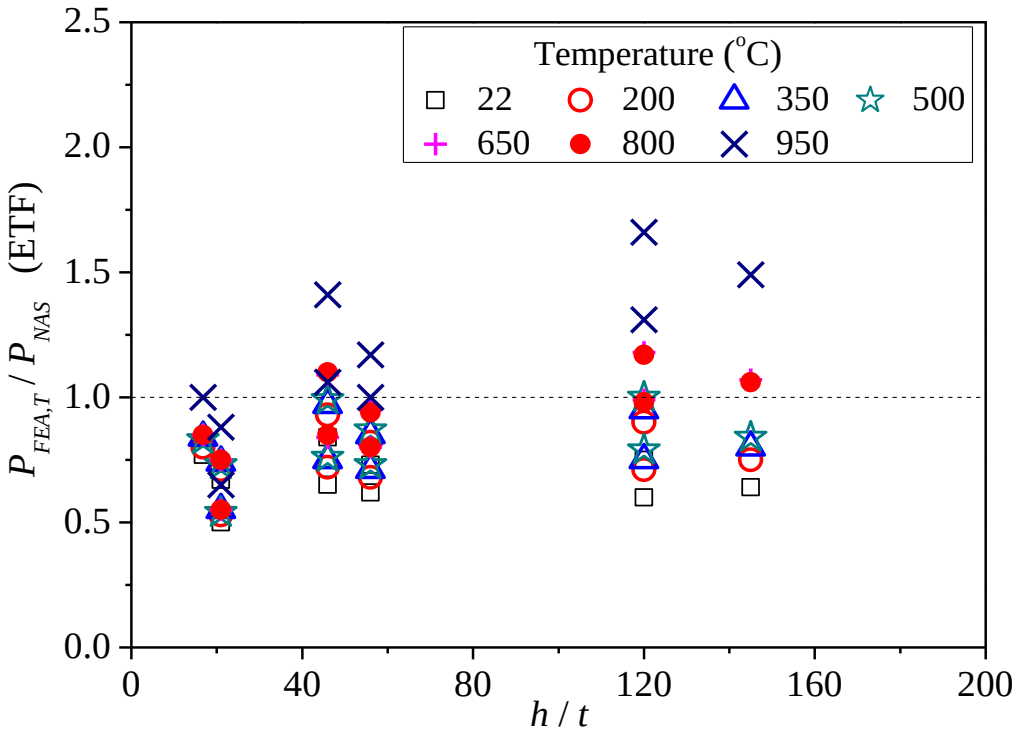

(c) NAS [39] for ETF

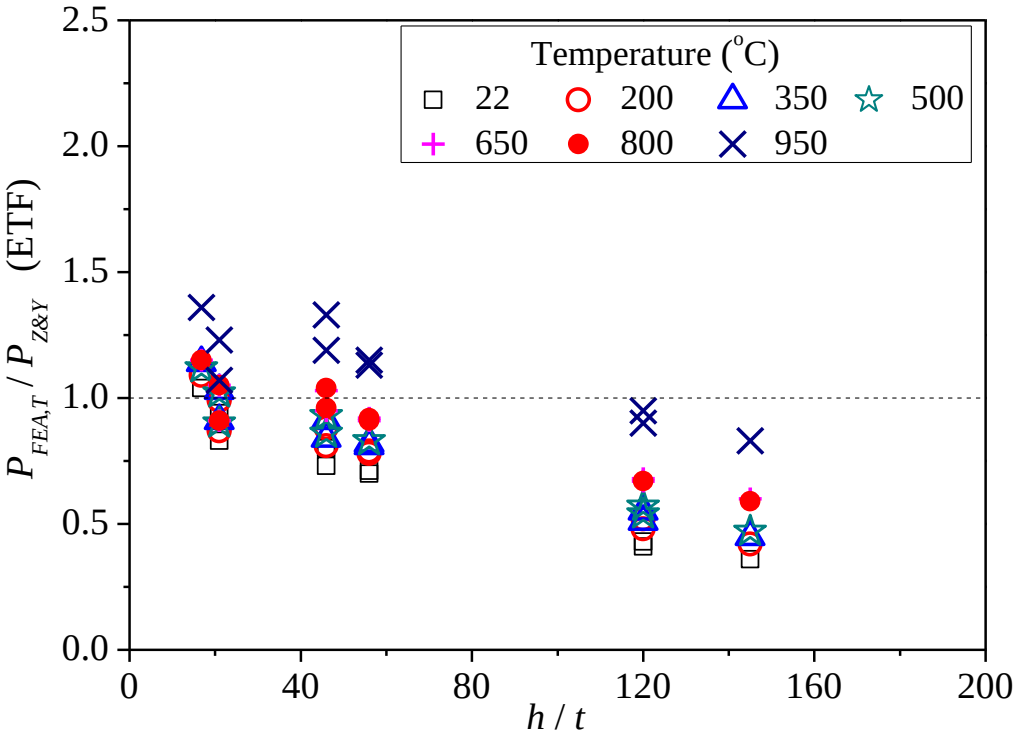

(d) Zhou and Young [30] for ETF

Figure 12: Comparison of FE results with current predictions for ETF loading condition

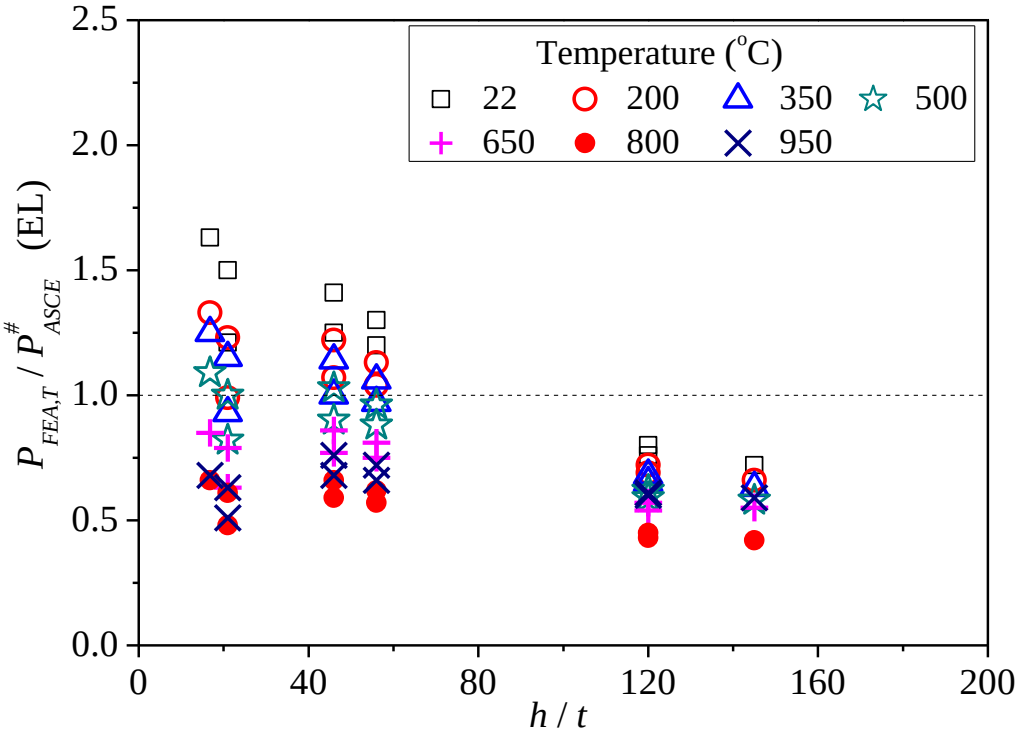

(a) Using ASCE EOF design rule [3] for EL

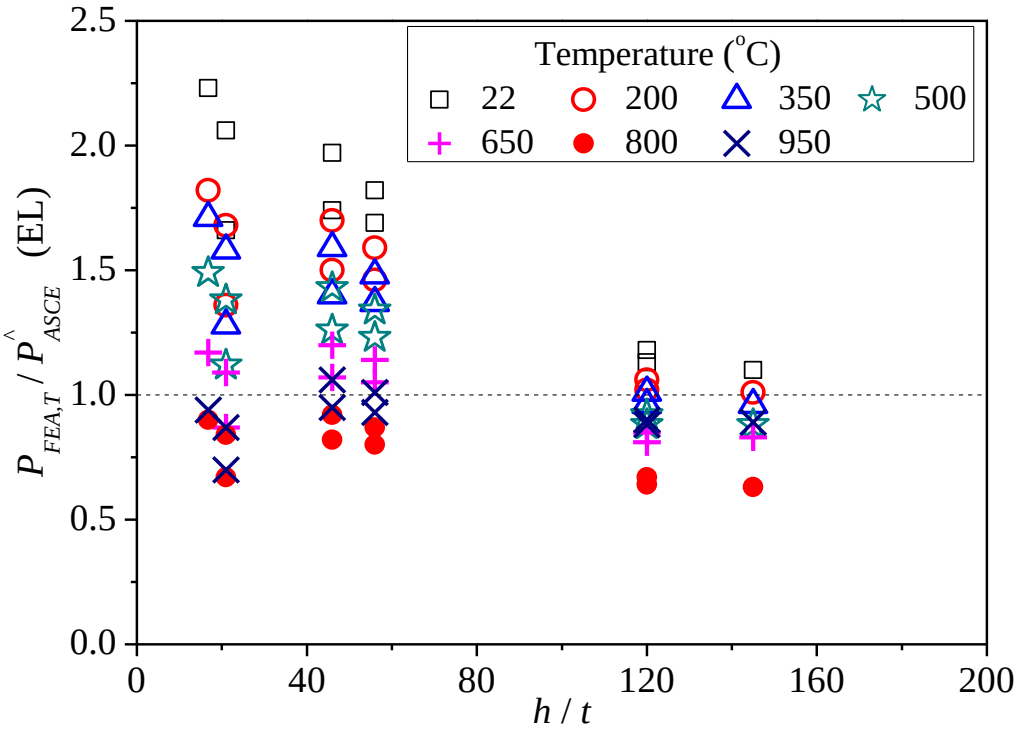

(b) Using ASCE ETF design rule [3] for EL

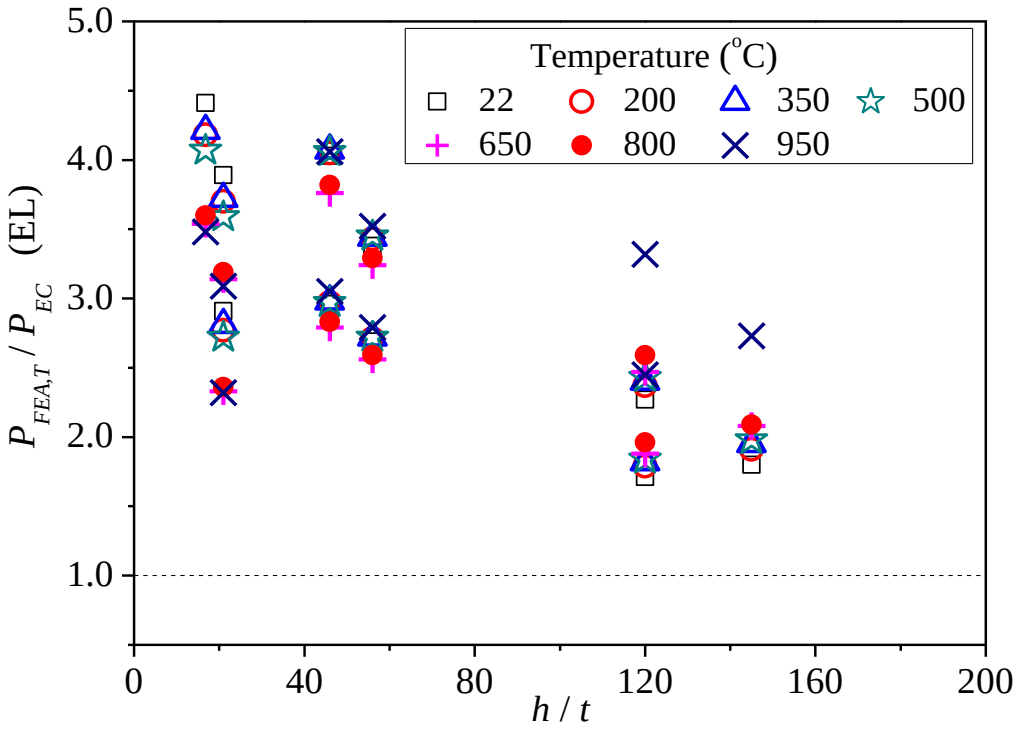

(c) Using EN 1993-1-3 [47] for EL

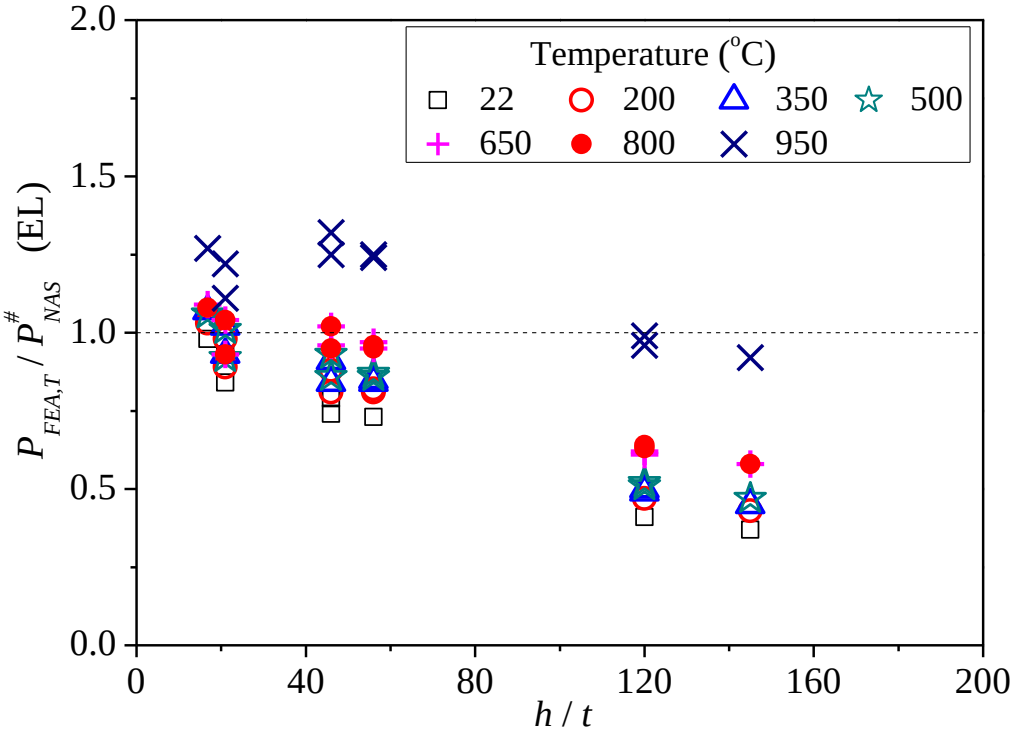

(d) Using NAS EOF design rule [39] for EL

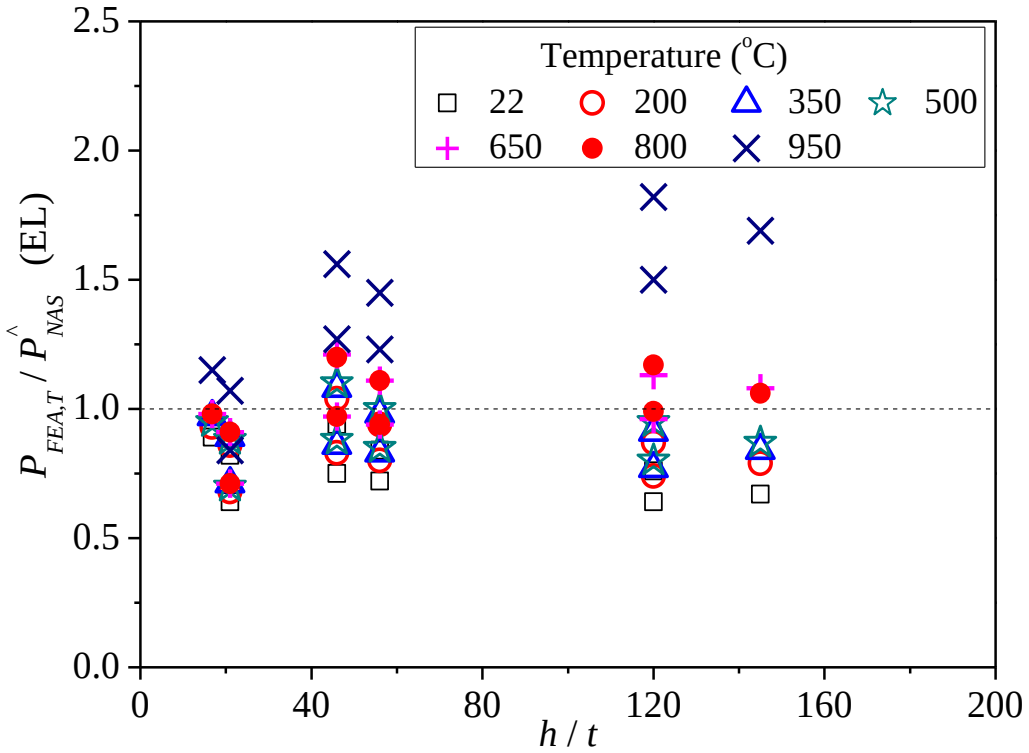

(e) Using NAS ETF design rule [39] for EL

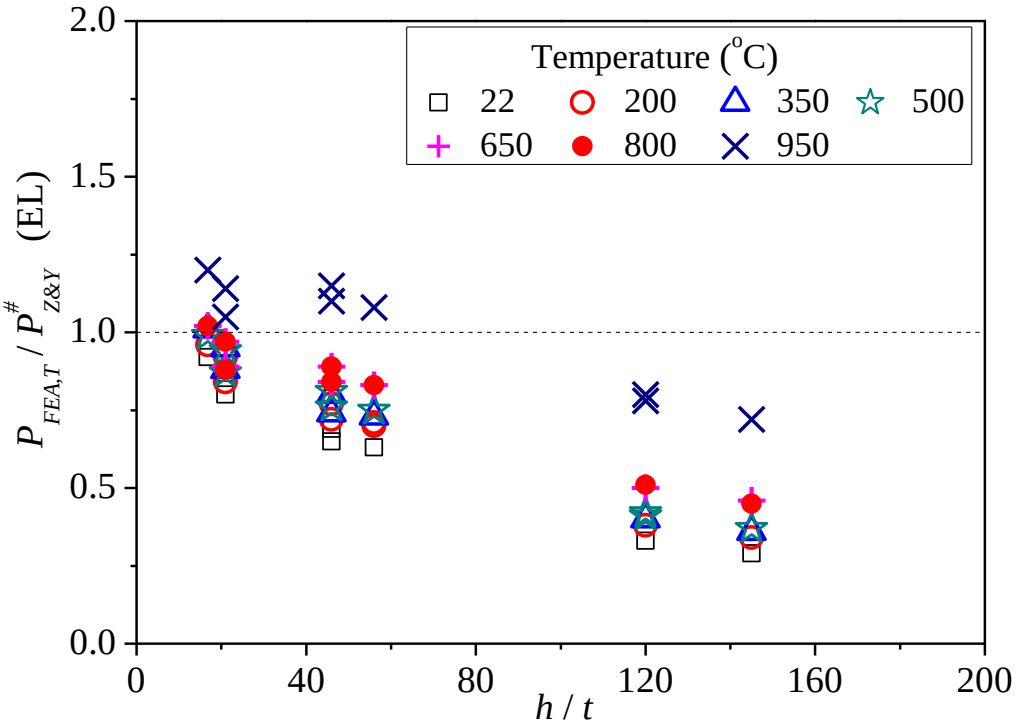

(f) Using Zhou and Young EOF coefficients [30] for EL

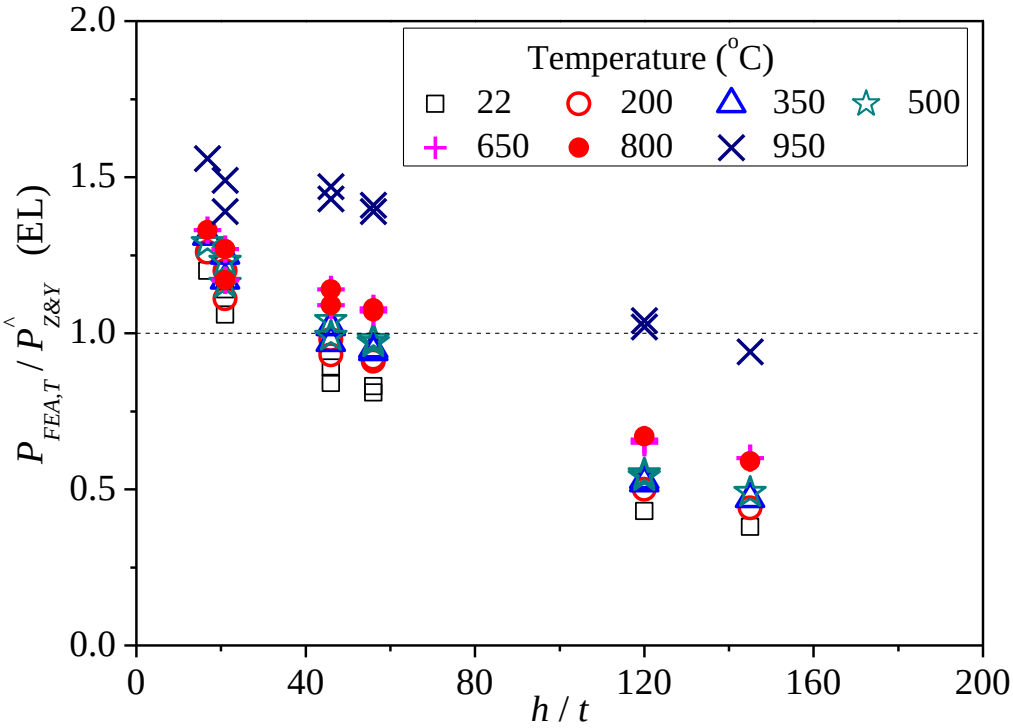

(g) Using Zhou and Young ETF coefficients [30] for EL

Figure 13: Comparison of FE results with current predictions for EL condition

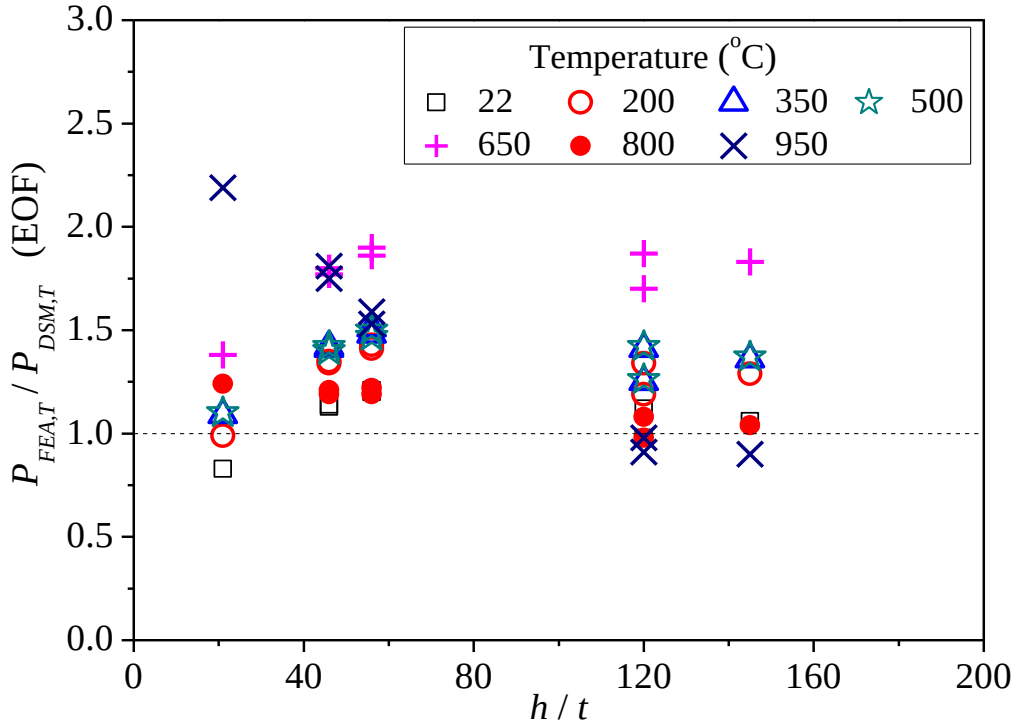

(a) Proposed predictions for EOF loading condition

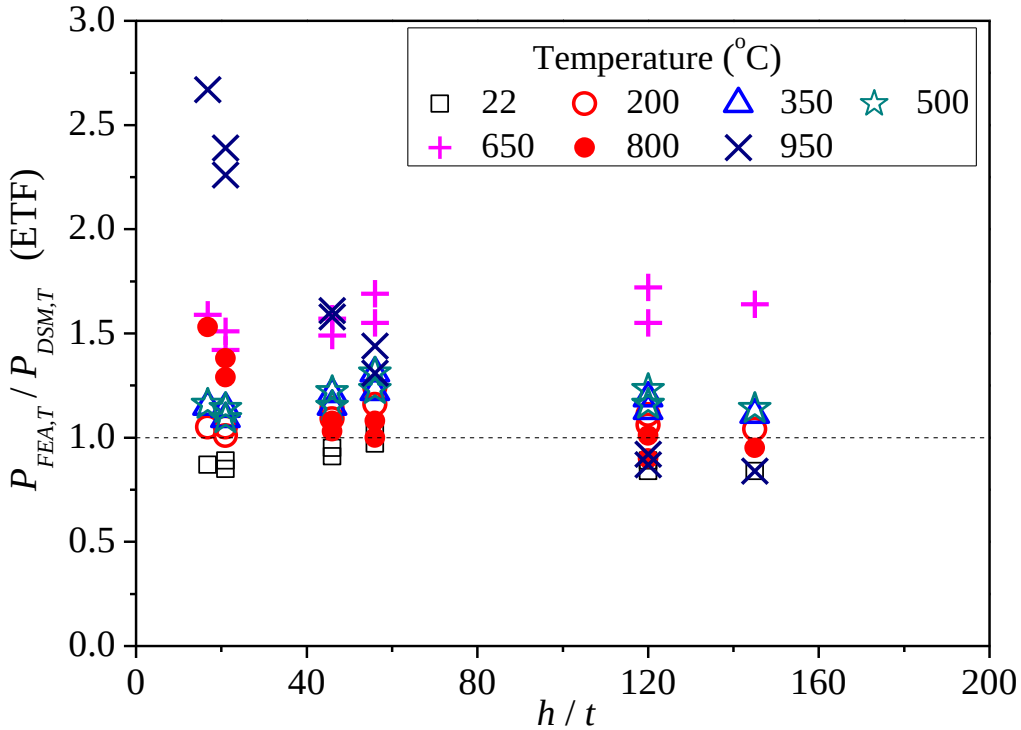

(b) Proposed predictions for ETF loading condition

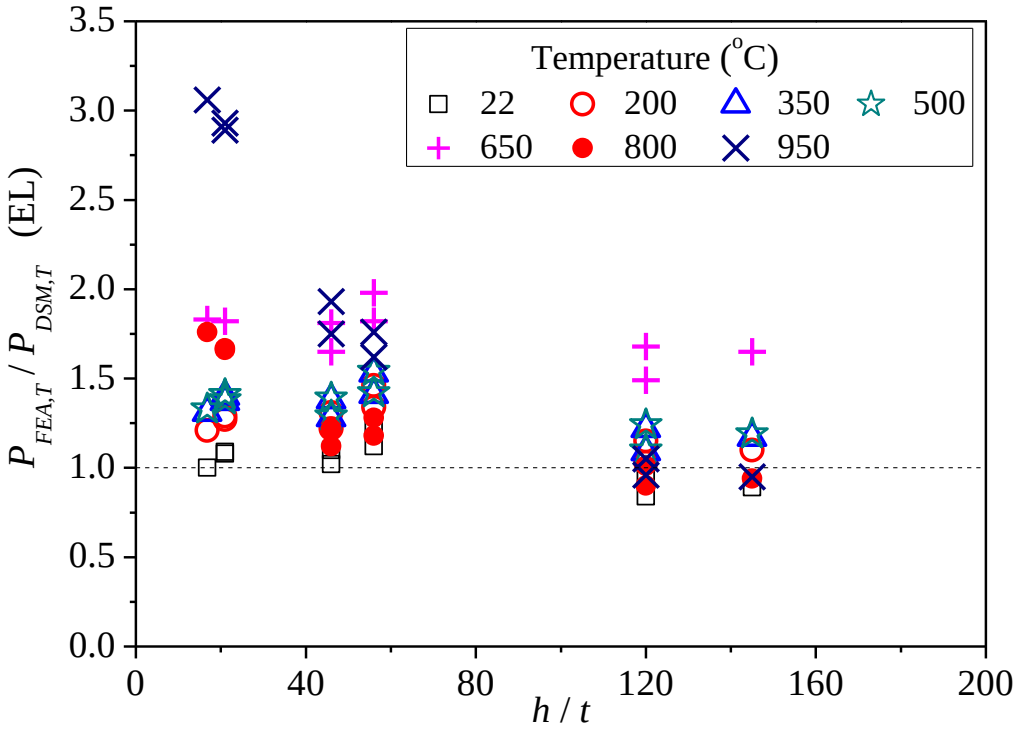

(c) Proposed predictions for EL condition

Figure 14: Comparison of FE results with proposed predictions for different loading conditions

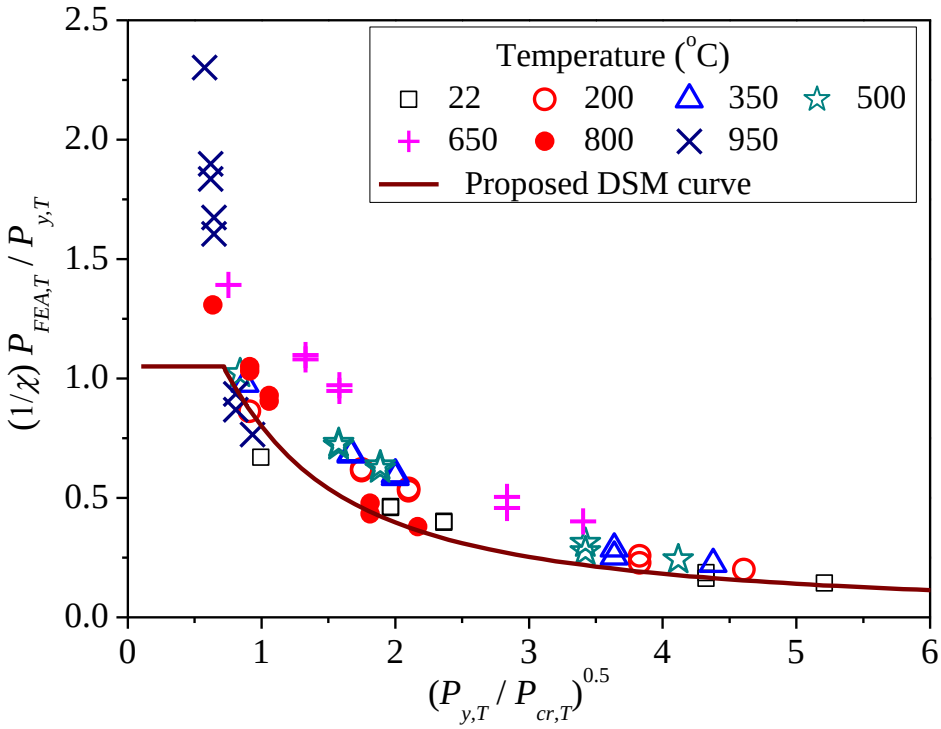

Figure 15: Comparison of FE results with modified DSM curve for EOF loading condition

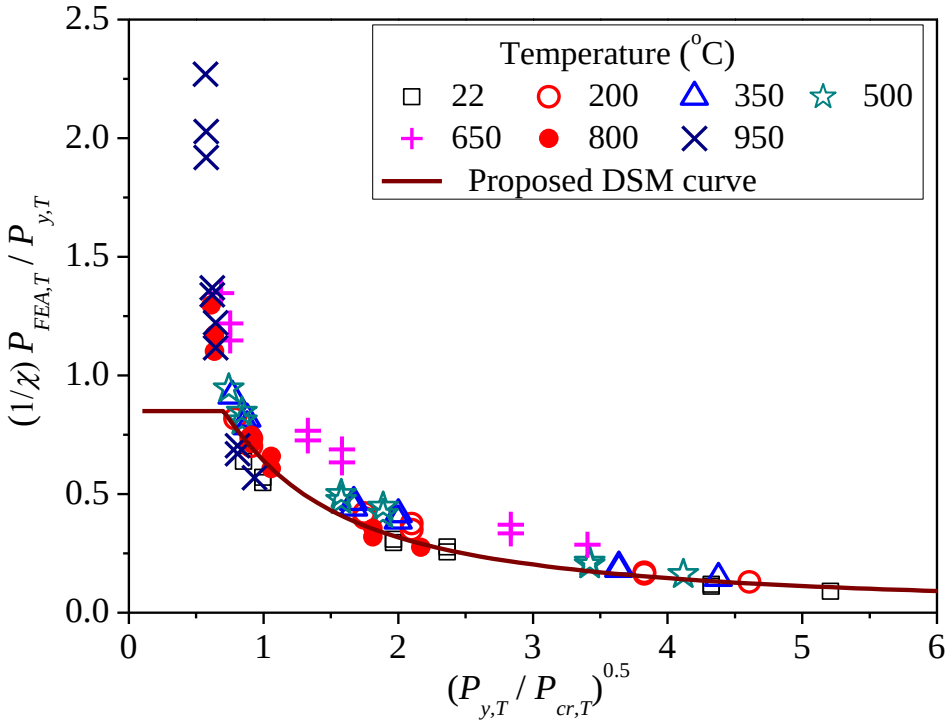

Figure 16: Comparison of FE results with modified DSM curve for ETF loading condition

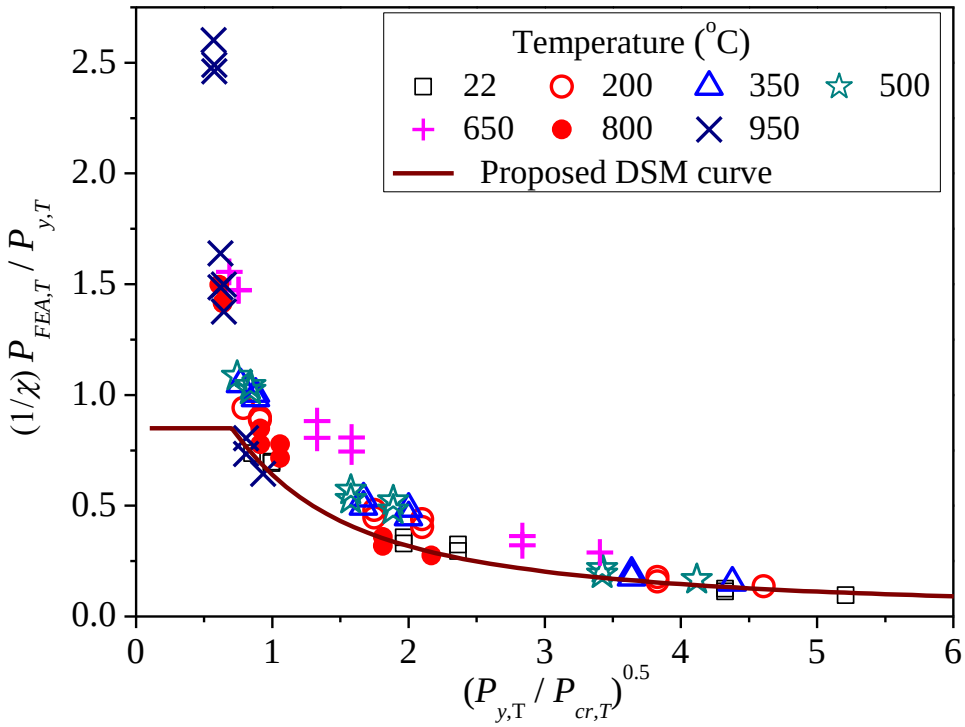

Figure 17: Comparison of FE results with modified DSM curve for EL condition

Table 1: Material properties of CFLDSS (EN 1.4062) at room temperature [37]

Section $H \times B \times t$ (mm)	E_r GPa	$f_{0.2,r}$ MPa	$f_{u,r}$ MPa
60×40×2.0	199	600	756
60×120×3.0	206	620	736
80×150×3.0	194	491	722
100×100×3.0	202	557	701
120×60×3.0	206	620	736
150×80×3.0	194	491	722

1155
1156 **Table 2:** Comparison of test strengths per web [37] with FE predictions

Specimen labelling	P_t (kN)	$P_{FEA,r}$ (kN)	$P_t/P_{FEA,r}$
EOF60×120×3.0N60	48.9	48.7	1.00
EOF80×150×3.0N60	35.7	32.2	1.11
EOF80×150×3.0N90	42.7	41.0	1.04
EOF100×100×3.0N30	39.6	29.7	1.33
EOF120×60×3.0N30	34.3	29.5	1.16
EOF120×60×3.0N60	46.7	46.3	1.01
EOF150×80×3.0N30	23.6	20.7	1.14
EOF150×80×3.0N90	37.3	36.2	1.03
ETF60×40×2.0N30	13.2	13.2	1.00
ETF60×40×2.0N30-r	13.9	13.2	1.05
ETF60×120×3.0N60	44.5	41.5	1.07
ETF60×120×3.0N90	56.7	53.8	1.05
ETF80×150×3.0N60	24.1	22.6	1.07
ETF80×150×3.0N150	44.3	41.6	1.06
ETF100×100×3.0N30	25.1	23.1	1.09
ETF100×100×3.0N90	42.4	39.0	1.09
ETF100×100×3.0N90-r	43.5	40.0	1.09
ETF120×60×3.0N30	24.5	25.1	0.98
ETF120×60×3.0N60	29.9	34.0	0.88
ETF150×80×3.0N30	19.2	16.9	1.14
ETF150×80×3.0N90	27.2	26.0	1.05
EL60×40×2.0N30	17.6	18.7	0.94
EL60×40×2.0N50	22.0	23.4	0.94
EL60×120×3.0N60	51.9	47.8	1.09
EL60×120×3.0N120	74.7	67.3	1.11
EL80×150×3.0N60	33.2	30.9	1.07
EL80×150×3.0N150	49.9	50.1	1.00
EL100×100×3.0N30	33.3	31.1	1.07
EL100×100×3.0N90	48.2	47.3	1.02
EL100×100×3.0N90-r	47.8	49.8	0.96
EL120×60×3.0N30	31.4	32.1	0.98
EL120×60×3.0N60	38.7	42.5	0.91
EL120×60×3.0N60-r	36.6	43.2	0.85
EL150×80×3.0N30	24.8	25.4	0.98
EL150×80×3.0N90	32.5	33.5	0.97
EL150×80×3.0N90-r	33.2	33.6	0.99

Table 3: Summary of comparisons of test strengths [37] with FE predictions

Loading condition	Number		$P_t/P_{FEA,r}$
EOF	8	Mean	1.10
		COV	0.100
ETF	13	Mean	1.05
		COV	0.061
EL	15	Mean	0.99
		COV	0.072
EOF, ETF and EL	36	Mean	1.04
		COV	0.086

Table 4: Design of CFLDSS specimens for parametric study at elevated temperatures

Section (H×B×t)	H (mm)	B (mm)	t (mm)	N (mm)	r/t	N/t	h/t	N/h
250×250×2.0	250	250	2.0	250	1.5	125.0	120.0	0.52
250×250×2.0	250	250	2.0	125	1.5	62.5	120.0	1.04
250×250×5.0	250	250	5.0	250	1.0	50.0	46.0	0.54
250×250×5.0	250	250	5.0	125	1.0	25.0	46.0	1.09
250×250×2.0	250	250	12.0	250	1.0	20.8	16.8	1.24
300×200×2.0	300	200	2.0	200	1.5	100.0	145.0	0.69
300×200×5.0	300	200	5.0	200	1.0	40.0	56.0	0.36
300×200×5.0	300	200	5.0	100	1.0	20.0	56.0	0.71
300×200×12.0	300	200	12.0	200	1.0	16.7	21.0	0.40
300×200×12.0	300	200	12.0	100	1.0	8.3	21.0	0.79

Table 5: Material properties of CFLDSS (EN 1.4162) steel at elevated temperatures [26]

Material properties	Nominal Temperature (°C)						
	22[#]	200	350	500	650	800	950
E_T (GPa)	200	190	183	169	160	60.4	13.5
$f_{0.2,T}$ (MPa)	724	564	508	448	393	304	119
$f_{u,T}$ (MPa)	862	710	696	627	514	358	138

Note: "[#]" room temperature.

Table 6: Web crippling strength per web of CFLDSS specimens at elevated temperatures

Specimen	Load at different temperature levels (kN)						
	22# °C	200 °C	350 °C	500 °C	650 °C	800 °C	950 °C
EOF250×250×2.0N125	17.0	15.0	14.1	12.8	10.1	3.9	0.8
EOF250×250×2.0N250	22.1	19.6	18.5	16.9	13.6	5.2	1.1
EOF250×250×5.0N125	140.1	119.6	111.9	99.3	72.7	28.2	5.1
EOF250×250×5.0N250	208.1	178.2	166.2	148.5	108.8	42.2	7.8
EOF250×250×12.0N250*	697.7	562.1	535.7	461.7	308.0	119.6	21.1
EOF300×200×2.0N200	18.0	16.1	15.2	13.8	11.2	4.3	0.9
EOF300×200×5.0N100	121.3	103.2	96.5	85.9	63.8	24.7	4.5
EOF300×200×5.0N200	168.9	145.0	135.4	120.9	90.1	35.0	6.4
EOF300×200×12.0N100	529.8	435.7	416.3	365.9	242.7	92.5	16.7
EOF300×200×12.0N200*	751.4	605.6	582.0	503.5	329.4	128.0	22.7
ETF250×250×2.0N125	10.8	9.9	9.5	8.8	7.4	2.9	0.6
ETF250×250×2.0N250	15.1	14.0	13.4	12.4	10.0	3.9	0.8
ETF250×250×5.0N125	94.4	81.9	76.5	69.0	51.7	20.4	3.8
ETF250×250×5.0N250	132.7	114.4	107.1	96.3	72.0	28.7	5.5
ETF250×250×12.0N250	724.9	593.3	559.5	486.1	337.6	131.9	23.6
ETF300×200×2.0N200	11.4	10.4	10.0	9.2	8.0	3.1	0.7
ETF300×200×5.0N100	84.6	73.1	68.1	61.5	46.4	18.0	3.4
ETF300×200×5.0N200	107.8	93.9	87.7	79.0	58.8	22.8	4.3
ETF300×200×12.0N100	433.2	354.2	334.3	290.2	200.2	77.9	13.9
ETF300×200×12.0N200	609.4	500.2	469.7	409.0	287.0	111.8	19.8
EL250×250×2.0N125	11.4	10.3	9.7	8.9	7.3	2.9	0.7
EL250×250×2.0N250	15.2	13.6	12.9	11.7	9.6	3.9	0.9
EL250×250×5.0N125	108.8	93.8	87.6	79.0	59.4	23.2	4.6
EL250×250×5.0N250	148.0	128.0	119.8	107.8	80.0	31.2	6.1
EL250×250×12.0N250	837.5	683.6	641.8	559.1	390.0	152.3	27.1
EL300×200×2.0N200	12.0	11.0	10.4	9.6	8.0	3.1	0.7
EL300×200×5.0N100	98.9	85.6	80.0	72.2	54.4	21.2	4.2
EL300×200×5.0N200	124.3	108.3	101.3	91.6	69.0	26.9	5.3
EL300×200×12.0N100	552.9	453.3	428.1	373.9	257.1	100.1	18.0
EL300×200×12.0N200	738.8	604.9	566.4	494.1	346.6	135.3	24.1

Note: "#" room temperature; "*" specimen failed in shear, but not web crippling.

Table 7: Coefficients for web crippling strength in the unified design equation

Resources	Loading condition	Coefficients					Limits ($\theta = 90^{\circ}$)			
		C	C_R	C_N	C_h	ϕ	r/t	N/t	h/t	N/h
NAS [39]	EOF	4.0	0.14	0.35	0.02	0.80	≤ 5.0	≤ 210	≤ 200	≤ 2.0
	ETF	13.0	0.32	0.05	0.04	0.90	≤ 3.0	≤ 210	≤ 200	≤ 2.0
Zhou and Young [30]	EOF	4.0	0.24	0.41	0.02	0.70	≤ 5.5	≤ 100	≤ 87	≤ 1.6
	ETF	3.0	0.30	0.48	0.03	0.70	≤ 5.5	≤ 100	≤ 87	≤ 1.6

Table 8: Comparison of test strengths [37] and FE predictions with predicted strengths at elevated temperatures for EOF loading condition

Temp. (°C)		$P_{FEA,T}/P_{ASCE}$	$P_{FEA,T}/P_{EC}$	$P_{FEA,T}/P_{NAS}$	$P_{FEA,T}/P_{Z\&Y}$	$P_{FEA,T}/P_{DSM,T}$
22[#]	Mean	1.42	3.59	0.81	0.70	1.09
	COV	0.238	0.299	0.257	0.289	0.116
200	Mean	1.22	3.60	0.90	0.77	1.29
	COV	0.230	0.294	0.244	0.275	0.111
350	Mean	1.15	3.62	0.94	0.81	1.37
	COV	0.224	0.288	0.239	0.271	0.099
500	Mean	1.03	3.60	0.95	0.82	1.37
	COV	0.219	0.286	0.232	0.263	0.094
650	Mean	0.87	3.37	1.05	0.90	1.76
	COV	0.208	0.277	0.207	0.231	0.096
800	Mean	0.66	3.38	1.03	0.88	1.15
	COV	0.214	0.282	0.213	0.237	0.085
950	Mean	0.74	3.50	1.29	1.11	1.46
	COV	0.197	0.271	0.180	0.199	0.330
All conditions	Mean	1.01	3.52	0.99	0.85	1.35
	COV	0.333	0.271	0.253	0.273	0.217
	Resistance factor, ϕ	0.70	0.91	0.80	0.70	0.80
	Reliability index, β	2.12	4.99	2.07	1.94	3.19

Note: "[#]" room temperature.

Table 9: Comparison of test strengths [37] and FE predictions with predicted strengths at elevated temperatures for ETF loading condition

Temp. (°C)		$P_{FEA,T}/P_{ASCE}$	$P_{FEA,T}/P_{EC}$	$P_{FEA,T}/P_{NAS}$	$P_{FEA,T}/P_{Z\&Y}$	$P_{FEA,T}/P_{DSM,T}$
22[#]	Mean	1.45	2.63	0.68	0.69	0.91
	COV	0.207	0.285	0.143	0.330	0.074
200	Mean	1.25	2.63	0.76	0.76	1.10
	COV	0.176	0.26	0.153	0.291	0.064
350	Mean	1.18	2.66	0.79	0.80	1.17
	COV	0.170	0.253	0.153	0.287	0.053
500	Mean	1.06	2.64	0.81	0.81	1.18
	COV	0.156	0.239	0.163	0.266	0.054
650	Mean	0.90	2.48	0.91	0.89	1.57
	COV	0.123	0.203	0.204	0.205	0.057
800	Mean	0.69	2.52	0.91	0.89	1.12
	COV	0.129	0.209	0.205	0.208	0.182
950	Mean	0.78	2.63	1.16	1.11	1.59
	COV	0.132	0.204	0.263	0.159	0.413
All conditions	Mean	1.04	2.60	0.86	0.85	1.23
	COV	0.295	0.229	0.260	0.275	0.282
	ϕ	0.70	0.91	0.90	0.70	0.80
	β	2.38	4.57	1.31	1.92	2.54

Note: "#" room temperature.

Table 10: Comparison of test strengths [37] and FE predictions with predicted strengths at elevated temperatures for EL condition

Temp. (°C)		$P_{FEA,T}/P^{\#}_{ASCE}$	$P_{FEA,T}/P^{\wedge}_{ASCE}$	$P_{FEA,T}/P_{EC}$	$P_{FEA,T}/P^{\#}_{NAS}$	$P_{FEA,T}/P^{\wedge}_{NAS}$	$P_{FEA,T}/P^{\#}_{Z\&Y}$	$P_{FEA,T}/P^{\wedge}_{Z\&Y}$	$P_{FEA,T}/P_{DSM,T}$
22#	Mean	1.18	1.66	3.00	0.69	0.77	0.61	0.80	1.03
	COV	0.268	0.240	0.308	0.321	0.134	0.371	0.372	0.112
200	Mean	1.01	1.42	2.99	0.76	0.85	0.67	0.88	1.24
	COV	0.239	0.211	0.281	0.290	0.125	0.339	0.339	0.101
350	Mean	0.95	1.33	3.01	0.79	0.88	0.70	0.91	1.32
	COV	0.235	0.207	0.278	0.287	0.122	0.337	0.337	0.100
500	Mean	0.85	1.19	2.98	0.80	0.90	0.71	0.92	1.33
	COV	0.222	0.194	0.266	0.272	0.123	0.321	0.321	0.097
650	Mean	0.71	1.01	2.78	0.88	1.00	0.77	1.01	1.75
	COV	0.177	0.152	0.226	0.221	0.140	0.269	0.267	0.079
800	Mean	0.55	0.78	2.83	0.88	1.00	0.77	1.01	1.28
	COV	0.172	0.146	0.222	0.215	0.143	0.263	0.262	0.247
950	Mean	0.64	0.91	3.08	1.15	1.36	1.01	1.32	1.89
	COV	0.112	0.103	0.174	0.128	0.221	0.173	0.169	0.433
All conditions	Mean	0.84	1.19	2.95	0.85	0.97	0.75	0.98	1.40
	COV	0.332	0.313	0.246	0.281	0.243	0.317	0.316	0.312
	ϕ	0.70	0.70	0.91	0.80	0.90	0.70	0.70	0.80
	β	1.68	2.61	4.78	1.54	1.70	1.45	2.11	2.71

Note: "#" room temperature.

Table 11: Coefficients for web crippling strength of CFLDSS by modified DSM at elevated temperatures

Loading condition	a	b	n	λ_k	γ	ϕ
EOF	1.00	0.20	0.60	0.720	1.05	0.80
ETF	0.80	0.20	0.60	0.700	0.85	0.80
EL	0.80	0.20	0.60	0.700	0.85	0.80

Note: The table is suitable to stiffened or partially stiffened flanges that unfastened to support; the proposed coefficients apply when $10 \leq h/t \leq 145$, $r_i/t \leq 1.5$, $N/t \leq 150$, $N/h \leq 1.5$ and $\theta = 90^{\circ}$.

Table 12: Comparison of test strengths [37] with modified DSM predictions for EOF loading condition at room temperature

Specimen labelling	h/t	r/t	N/t	N/h	P_t (kN)	$P_{DSM,T}$ (kN)	$P_t/P_{DSM,T}$
EOF60×120×3.0N60	15.7	0.9	19.5	1.25	48.9	50.4	0.97
EOF80×150×3.0N60	19.8	2.1	19.5	0.98	35.7	23.0	1.48
EOF80×150×3.0N90	20.0	2.1	29.1	1.46	42.7	29.1	1.40
EOF100×100×3.0N30	28.4	1.1	9.7	0.34	39.6	26.0	1.52
EOF120×60×3.0N30	35.0	1.1	9.8	0.28	34.3	28.0	1.23
EOF120×60×3.0N60	35.2	0.9	19.5	0.56	46.7	37.4	1.25
EOF150×80×3.0N30	42.8	2.1	9.7	0.23	23.6	16.5	1.43
EOF150×80×3.0N90	42.9	2.0	29.1	0.68	37.3	25.1	1.48
						Mean	1.35
						COV	0.139
						Resistance factor, ϕ	0.80
						Reliability index, β	3.51

Table 13: Comparison of test strengths [37] with modified DSM predictions for ETF loading condition at room temperature

Specimen labelling	*h/t*	*r/t*	*N/t*	*N/h*	P_t (kN)	$P_{DSM,T}$ (kN)	$P_t/P_{DSM,T}$
ETF20×50×1.5N30	10.2	0.6	20.1	1.97	18.0	13.7	1.31
ETF20×50×1.5N50	10.1	0.6	33.5	3.32	28.7	19.5	1.47
ETF40×60×2.0N30	16.4	0.9	15.1	0.92	16.4	14.1	1.16
ETF40×60×2.0N60	16.1	1.1	30.0	1.87	24.8	21.1	1.17
ETF40×60×2.0N60-r	16.3	1.0	30.2	1.85	25.1	21.3	1.18
ETF50×20×1.5N30	30.1	0.5	19.8	0.66	9.9	10.4	0.95
ETF60×40×2.0N30	26.2	0.9	15.0	0.57	13.2	12.5	1.05
ETF60×40×2.0N30-r	26.2	0.9	15.0	0.57	13.9	12.5	1.11
ETF60×120×3.0N60	15.7	0.9	19.6	1.25	44.5	40.1	1.11
ETF60×120×3.0N90	15.6	0.9	29.3	1.88	56.7	52.6	1.08
ETF80×150×3.0N60	20.0	2.1	19.5	0.97	24.1	23.0	1.23
ETF80×150×3.0N150	19.9	2.1	48.6	2.44	44.3	41.1	1.27
ETF100×100×3.0N30	28.4	1.1	9.7	0.34	25.1	20.5	1.22
ETF100×100×3.0N90	28.3	1.1	29.2	1.03	42.4	34.4	1.23
ETF100×100×3.0N90-r	28.4	1.0	29.1	1.02	43.5	35.2	1.24
ETF120×60×3.0N30	34.9	1.1	9.7	0.28	24.5	22.7	1.08
ETF120×60×3.0N60	35.2	0.9	19.5	0.55	29.9	29.9	1.00
ETF150×80×3.0N30	42.6	2.1	9.7	0.23	19.2	13.2	1.46
ETF150×80×3.0N90	43.0	2.0	29.2	0.68	27.2	19.9	1.37
						Mean	1.19
						COV	0.119
						Resistance factor, ϕ	0.80
						Reliability index, β	3.38

Table 14: Comparison of test strengths [37] with modified DSM predictions for EL condition at room temperature

Specimen labelling	*h/t*	*r/t*	*N/t*	*N/h*	P_t (kN)	$P_{DSM,T}$ (kN)	$P_t/P_{DSM,T}$
EL20×50×1.5N30	9.8	0.7	19.8	2.03	20.7	12.9	1.60
EL20×50×1.5N50	10.0	0.6	32.7	3.27	29.3	20.4	1.43
EL40×60×2.0N30	16.5	0.8	14.9	0.91	19.9	14.9	1.34
EL40×60×2.0N60	16.6	0.8	30.0	1.81	29.6	22.7	1.30
EL50×20×1.5N30	29.4	0.7	19.7	0.67	12.1	9.8	1.23
EL60×40×2.0N30	26.4	0.7	14.9	0.56	17.6	13.4	1.31
EL60×40×2.0N50	26.0	0.8	24.5	0.94	22.0	17.5	1.25
EL60×120×3.0N60	15.8	0.9	19.5	1.24	51.9	40.3	1.29
EL60×120×3.0N120	15.6	1.0	39.0	2.49	74.7	64.3	1.16
EL80×150×3.0N60	20.1	1.9	19.4	0.97	33.2	24.3	1.61
EL80×150×3.0N150	20.2	2.0	48.6	2.41	49.9	42.9	1.37
EL100×100×3.0N30	28.1	1.2	9.7	0.35	33.3	20.2	1.65
EL100×100×3.0N90	27.8	1.3	29.1	1.05	48.2	32.9	1.46
EL100×100×3.0N90-r	28.4	1.1	29.2	1.03	47.8	34.2	1.40
EL120×60×3.0N30	34.7	1.0	9.7	0.28	31.4	23.1	1.36
EL120×60×3.0N60	35.0	1.0	19.5	0.56	38.7	29.4	1.32
EL120×60×3.0N60-r	35.1	0.9	19.5	0.56	36.6	30.1	1.22
EL150×80×3.0N30	43.2	1.9	9.7	0.23	24.8	13.5	1.83
EL150×80×3.0N90	43.5	1.9	29.2	0.67	32.5	19.9	1.63
EL150×80×3.0N90-r	43.2	1.9	29.2	0.68	33.2	20.0	1.66
						Mean	1.42
						COV	0.129
						Resistance factor, ϕ	0.80
						Reliability index, β	3.95